

EFFECTS OF MODELING METHODS ON THE FINITE ELEMENT ANALYSIS  
RESULTS OF ORTHODONTIC APPLICATIONS

A Thesis

Submitted to the Faculty

of

Purdue University

by

Yanzhi Liu

In Partial Fulfillment of the

Requirements for the Degree

of

Master of Science in Mechanical Engineering

December 2017

Purdue University

Indianapolis, Indiana

**THE PURDUE UNIVERSITY GRADUATE SCHOOL**  
**STATEMENT OF COMMITTEE APPROVAL**

Dr. Jie Chen, Chair

Department of Mechanical Engineering

Dr. Diane Wagner

Department of Mechanical Engineering

Dr. Hazim El-Mounayri

Department of Mechanical Engineering

**Approved by:**

Dr. Jie Chen

Head of the Graduate Program

I would like to dedicate my thesis to my beloved parents and all my friends who help me through this.

## ACKNOWLEDGMENTS

I would like to thank my advisers, Professors Chen Jie and my senior lab mate Jiang Feifei, for their guidance, support and trust throughout the completion of this work. The year that is conveyed in the succeeding pages has been one of the most significant eras of my personal life, for which I will always be grateful. In retrospect, it is plainly clear to me that, having discovered a sincere desire to explore the unknown, I am all only better because of it.

I would like to thank the Purdue University Department of Mechanical Engineering, for the opportunity to let me, an international student, be a part of this campus and learn a lot of interesting stuff which I can apply to my thesis research.

Finally, I would like to thank my family and friends, who over the past years have quietly missed me and patiently endured my perpetual droning on about strains, singularities and what interesting things teeth do.

## TABLE OF CONTENTS

	Page
LIST OF TABLES . . . . .	ix
LIST OF FIGURES . . . . .	x
ABSTRACT . . . . .	xiv
1 INTRODUCTION . . . . .	1
1.1 Malocclusion and the Solution . . . . .	1
1.2 Tooth Structure and Importance of Tooth Movement Algorithm . . . . .	2
1.3 Finite Element Method and Cone-beam Computed Tomography . . . . .	4
1.3.1 CBCT Limitations . . . . .	5
1.4 Initial Displacement and Stress . . . . .	5
1.5 Space Closure in Orthodontic Treatment . . . . .	7
1.6 Knowledge Gap . . . . .	9
1.6.1 Previous Relevant Work . . . . .	9
1.6.2 Types of Boundary Conditions . . . . .	11
1.7 Research Objectives . . . . .	12
2 MATERIALS AND METHODOLOGY . . . . .	13
2.1 Overview . . . . .	13
2.2 Material . . . . .	13
2.3 Geometry Reconstruction . . . . .	13
2.3.1 3D Segmentation of the CBCT Scan . . . . .	13
2.3.2 Reconstruction of the Tooth, PDL and Cortical Bone . . . . .	15
2.4 Finite Element Modeling . . . . .	18
2.4.1 Geometry Assembly . . . . .	18
2.4.2 Material Properties . . . . .	19
2.5 Boundary Conditions . . . . .	20

	Page
2.5.1	1 <sup>st</sup> Model Set Up (Canine Retraction with Segmental T-Loop) . . . . . 22
2.5.2	2 <sup>nd</sup> Model Set Up (Canine Retraction with Power Arm) . . . . . 24
2.5.3	3 <sup>rd</sup> Model Set Up (En-masse Retraction with Flexible Wire) . . . . . 26
2.5.4	4 <sup>th</sup> Model Set Up (En-masse Retraction with Rigid Wire) . . . . . 26
2.5.5	5 <sup>th</sup> Model Set Up (En-masse Retraction with Power Arm Attached to the Archwire) . . . . . 27
2.6	Convergence Test . . . . . 28
3	RESULTS . . . . . 31
3.1	OBJ#1: To Build up a Reliable Model with Details . . . . . 31
3.2	OBJ #2: Comparison of the Simplified Model and Detailed Model . . . . . 32
3.2.1	Comparison of First Principal Stress in PDL . . . . . 32
3.2.2	Comparison of Second Principal Stress in PDL . . . . . 33
3.2.3	Comparison of Third Principal Stress in PDL . . . . . 34
3.2.4	Comparison of Von-Mises Stress in PDL . . . . . 35
3.2.5	Comparison of First Principal Stress in Cortical Bone . . . . . 37
3.2.6	Comparison of Second Principal Stress in Cortical Bone . . . . . 38
3.2.7	Comparison of Third Principal Stress in Cortical Bone . . . . . 39
3.2.8	Comparison of Von-Mises Stress in Cortical Bone . . . . . 40
3.2.9	Comparison of Tooth Displacement . . . . . 41
3.3	OBJ #3: Mechanical Environment Changes due to Different Treatments (Canine Retraction with T-Loop and Power Arm) . . . . . 42
3.3.1	First Principal Stress in PDL from Canine T-Loop Model . . . . . 43
3.3.2	Second Principal Stress in PDL from Canine T-Loop Model . . . . . 43
3.3.3	Third Principal Stress in PDL from Canine T-Loop Model . . . . . 44
3.3.4	Von-Mises Stress in PDL from Canine T-Loop Model . . . . . 44
3.3.5	First Principal Stress in Bone from Canine T-Loop Model . . . . . 45
3.3.6	Second Principal Stress in Bone from Canine T-Loop Model . . . . . 45
3.3.7	Third Principal Stress in Bone from Canine T-Loop Model . . . . . 46
3.3.8	Von-Mises Stress in Bone from Canine T-Loop Model . . . . . 46

	Page
3.3.9 Tooth Displacement from Canine T-Loop Model . . . . .	47
3.3.10 First Principal Stress in PDL from Canine Power arm Model . .	47
3.3.11 Second Principal Stress in PDL from Canine Power Arm Model	48
3.3.12 Third Principal Stress in PDL from Canine Power Arm Model .	48
3.3.13 Von-Mises Stress in PDL from Canine Power Arm Model . . . .	49
3.3.14 First Principal Stress in Bone from Canine Power Arm Model .	49
3.3.15 Second Principal Stress in Bone from Canine Power Arm Model	50
3.3.16 Third Principal Stress in Bone from Canine Power Arm Model .	50
3.3.17 Von-Mises Stress in Bone from Canine Power Arm Model . . . .	51
3.3.18 Tooth Displacement from Canine Power Arm Model . . . . .	51
3.3.19 First Principal Stress in PDL from En-masses Retraction (Power Arm on Wire) Model . . . . .	52
3.3.20 Second Principal Stress in PDL from En-masses Retraction (Power Arm on Wire) Model . . . . .	52
3.3.21 Third Principal Stress in PDL from En-masses Retraction (Power Arm on Wire) Model . . . . .	53
3.3.22 Von-Mises Stress in PDL from En-masses Retraction (Power Arm on Wire) Model . . . . .	53
3.3.23 First Principal Stress in Bone from En-masses Retraction (Power Arm on Wire) Model . . . . .	54
3.3.24 Second Principal Stress in Bone from En-masses Retraction (Power Arm on Wire) Model . . . . .	54
3.3.25 Third Principal Stress in Bone from En-masses Retraction (Power Arm on Wire) Model . . . . .	55
3.3.26 Von-Mises Stress in Bone from En-masses Retraction (Power Arm on Wire) Model . . . . .	55
3.3.27 Sliding Distance from En-masses Retraction (Power Arm on Wire) Model . . . . .	56
3.3.28 Tooth Displacement from En-masses Retraction (Power Arm on Wire) Model . . . . .	56
3.3.29 Wire Displacement from En-masses Retraction (Power Arm on Wire) Model . . . . .	57

	Page
4 DISCUSSION . . . . .	58
4.1 Overview . . . . .	58
4.2 Objective #1 . . . . .	58
4.3 Objective #2 . . . . .	58
4.4 Objective #3 . . . . .	60
4.4.1 Effects of Cantilever Location on the Mechanical Environment . . . . .	60
4.4.2 Mechanical Environment Change due to Segmental T-loop Used for Canine Retraction . . . . .	61
4.4.3 Mechanical Environment Change due to En-masse Retraction (Power Arm on Canine) . . . . .	62
5 CONCLUSION . . . . .	64
REFERENCES . . . . .	65

## LIST OF TABLES

Table	Page
2.1 Material Properties . . . . .	19
2.2 Model Descriptions . . . . .	22
3.1 The Results of Convergence Test . . . . .	32
3.2 Standard Deviation (STD) . . . . .	32
3.3 The Summary of Result Comparison from Simplified Model and Detailed Model . . . . .	42

## LIST OF FIGURES

Figure	Page
1.1 Tooth anatomic structure . . . . .	2
1.2 Tooth anatomic structure . . . . .	4
1.3 Custom-made segmental wire with T loop . . . . .	8
1.4 Power arm and implant in en-mass retraction . . . . .	8
1.5 Previous model for canine retraction with T-Loop [38] . . . . .	10
1.6 Previous model for en-masse retraction case . . . . .	10
1.7 Previous model for en-masse retraction case . . . . .	11
2.1 X, Y, Z axis in Mimics . . . . .	14
2.2 Teeth polylines(upperleft),alveolar bone polylines(lower left), selected teeth polylines(upper right),and selected alveolar bone polylines(lower right) . . . . .	15
2.3 Polylines in Creo (left); Sketch planes and spline lines (right) . . . . .	15
2.4 Final geometry of canine. It was consist of crown and root. . . . .	16
2.5 0.2mm offset spline line was set to generate PDL horizontally and vertically	17
2.6 Orthodontic wire and simplified bracket . . . . .	17
2.7 PDL (green, covered by bone) and cortical bone (transparent layer) . . . . .	18
2.8 Vertical sectional view of the model . . . . .	19
2.9 Final model overlook (for canine power arm case and en-masse retraction case) . . . . .	20
2.10 The boundary conditions of the half mandible model. (Tag C and D in yellow are displacement constrain and Tag A in blue is fixed constrain. Tag B in red is the applied force) . . . . .	21
2.11 Two contact types between wire and brackets . . . . .	22
2.12 Meshing overlook of canine (T loop) model . . . . .	23
2.13 Equivalent forces of T loop that were applied on bracket in canine T-Loop model . . . . .	24

Figure	Page
2.14 Meshing overlook of canine retraction (power arm) model . . . . .	25
2.15 Loading condition (Horizontal force in XY plane towards to implant) . . . . .	25
2.16 Meshing overlook and loading condition of en-masse retraction (flexible wire) model . . . . .	26
2.17 Meshing overlook and loading condition of en-masse retraction (rigid wire) model . . . . .	27
2.18 Remodeled wire of different cantilever location . . . . .	28
2.19 Meshing overlook and loading condition of en-masse retraction (power arm on wire) model . . . . .	28
2.20 The chosen targeted point for displacement in the convergence test . . . . .	29
2.21 The chosen targeted point for 3rd principal stress in the convergence test . . . . .	30
3.1 Comparison of first principal stress in PDL from detailed model and simplified model . . . . .	33
3.2 Comparison of second principal stress in PDL from detailed model and simplified model . . . . .	34
3.3 Comparison of third principal stress in PDL from detailed model and simplified model . . . . .	35
3.4 Comparison of von-Mises stress in PDL from detailed model and simplified model . . . . .	36
3.5 Comparison of first principal stress in bone from detailed model and simplified model . . . . .	37
3.6 Comparison of second principal stress in bone from detailed model and simplified model . . . . .	38
3.7 Comparison of third principal stress in bone from detailed model and simplified model . . . . .	39
3.8 Comparison of Von-Mises stress in bone from detailed model and simplified model . . . . .	40
3.9 Comparison of tooth displacement from detailed model and simplified model	41
3.10 First principal stress in PDL from canine T-Loop model . . . . .	43
3.11 Second principal stress in PDL from canine T-Loop model . . . . .	43
3.12 Third principal stress in PDL from canine T-Loop model . . . . .	44
3.13 Von-Mises stress in PDL from canine T-Loop model . . . . .	44

Figure	Page
3.14 First principal stress in bone from canine T-Loop Model . . . . .	45
3.15 Second principal stress in bone from canine T-Loop model . . . . .	45
3.16 Third principal stress in bone from canine T-Loop model . . . . .	46
3.17 Von-Mises stress in bone from canine T-Loop model . . . . .	46
3.18 Tooth Displacement from canine T-Loop model . . . . .	47
3.19 First principal stress in PDL from canine T-Loop model . . . . .	47
3.20 Second Principal stress in PDL from canine T-Loop model . . . . .	48
3.21 Third Principal stress in PDL from canine T-Loop model . . . . .	48
3.22 Von-Mises stress in PDL from canine T-Loop model . . . . .	49
3.23 First principal stress in bone from canine T-Loop model . . . . .	49
3.24 Second principal stress in bone from canine T-Loop model . . . . .	50
3.25 Third principal stress in bone from canine T-Loop model . . . . .	50
3.26 Von-Mises stress in bone from canine T-Loop model . . . . .	51
3.27 Tooth displacement from canine power arm model . . . . .	51
3.28 First principal stress in PDL from en-masses retraction (power arm on wire) model . . . . .	52
3.29 Second principal stress in PDL from en-masses retraction (power arm on wire) model . . . . .	52
3.30 Third principal stress in PDL from en-masses retraction (power arm on wire) model . . . . .	53
3.31 Von-Mises stress in PDL from en-masses retraction (power arm on wire) model . . . . .	53
3.32 First principal Stress in bone from en-masses retraction (power arm on wire) model . . . . .	54
3.33 Second principal stress in bone from en-masses retraction (power arm on wire) model . . . . .	54
3.34 Third principal stress in bone from en-masses retraction (power arm on wire) model . . . . .	55
3.35 Von-Mises stress in bone from en-masses retraction (power arm on wire) model . . . . .	55
3.36 Sliding distance from en-masses retraction (power arm on wire) model . .	56

Figure	Page
3.37 Tooth displacement from en-masses retraction (power arm on wire) model	56
3.38 Wire displacement from en-masses retraction (power arm on wire) model	57

## ABSTRACT

Liu, Yanzhi. M.S.M.E., Purdue University, December 2017. Effects of Modeling Methods on the Finite Element Analysis Results of Orthodontic Applications. Major Professor: Jie Chen.

Identification of the mechanical environment changes in the tissues due to implementation of various treatment strategies are important for understanding the mechanism of the treatment outcomes, evaluating design of orthodontic appliances, and design of new treatment strategies. The goal of this study is to develop a finite element model that can be used to reliably estimate the mechanical environment changes due to various orthodontic treatment. The objectives are: 1) to build up a reliable model with details that can be more reliably utilized to simulate different orthodontic clinical cases, which will help orthodontists to predict the treatment outcomes, 2) to assess the significance of the differences between the simplified model and the models with more details, and (3) to apply the technology to clinical cases and estimate mechanical environment changes. A finite element model was created based on cone beam computed tomography (CBCT) images of an anonymous volunteer. The bone and teeth were segmented first. The finite element models were created using the geometries. The models were unique because the interfaces between the neighboring crowns and between the archwire and brackets were modeled using the contact elements, which allowed more realistic representation of the interfaces. The element size was determined through a convergence test. The validity of the stress was judged based on the calculated stress distribution. Then, the results of the new model were compared with these from a simplified model representing the studies published previously. The purpose was to see whether the simplified model can be used to replace a detailed model. Three clinical treatment strategies were

modeled to evaluate the corresponding mechanical environment changes. The results showed that the new model produced more reasonable stress distribution than the simplified model. The simplified model resulted in much lower stress in the PDL than the detailed model, thus should not be used to quantify the stresses. The mechanical environment changes due to various treatment strategies provided useful information for studying the biological responses to the orthodontic load systems.

# 1. INTRODUCTION

## 1.1 Malocclusion and the Solution

Malocclusion is a common issue which could affect peoples lives globally. It is important to find effective treatments [1]. The term malocclusion refers to misalignment or improper relation between the upper teeth and lower teeth when they approach each other, referring to as bite. According to a research, there is 27.9% of United States population suffering from different severity levels of malocclusion and half of the teenagers face malocclusion problems as well as its treatment [2]. Usually malocclusion will affect peoples facial shape and development but the patients with a severe level of malocclusion suffer from a higher level of oral health trouble than those who do not [3].

Orthodontic treatment is for correction of malocclusion. The purpose of the treatment is to move the teeth in disarray to correct positions by using orthodontic appliance. The treatments from orthodontists include but not limit to skeletal surgery, alignment, space closure, etc. These are accomplished by appliances, such as archwire, brackets, implant, springs, and various ligation methods [4]. The primarily purpose of the appliances is to apply an adequate load system to the target teeth. The constraints are: treatment duration, treatment cost, devices replaceability, oral comfortability, and pain level, which may vary and have been concerned by both orthodontists and patients. It is imperative to be able to quantify and control the load system to optimize the treatment.

## 1.2 Tooth Structure and Importance of Tooth Movement Algorithm

Teeth can be moved under proper orthodontic load. The load triggers the tooth movement, but the movement is completed by biological response [5]. Figure 1.1 shows the anatomic structure of a tooth and its surrounding tissues. The tooth can be divided into two parts, the crown is the upper part which can be seen and the root is the lower part which is embedded in bone. The periodontal ligament (PDL), a thin membrane, is a soft tissue that separates and transmits orthodontic loads between root and bone. Alveolar bone is a hard tissue that forms the socket hosting the root and PDL. In general, a health root does not contact bone directly because the root is covered by the PDL [6].

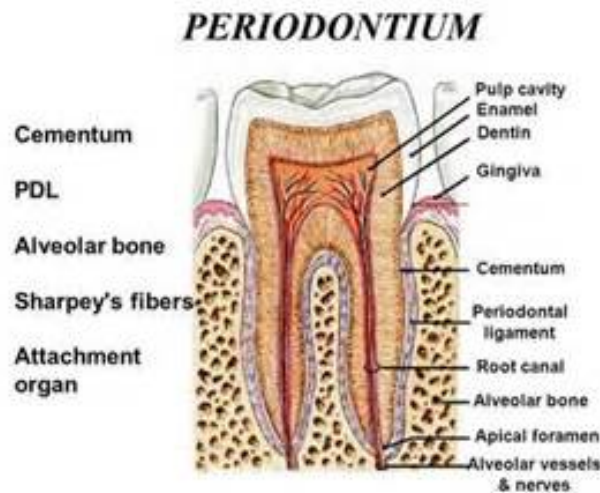


Fig. 1.1.: Tooth anatomic structure

Based on current researches, teeth move due to the stress in PDL generated by the orthodontic load [6]. There are many types of cells and matrix in PDL. Two of them, which play critical roles in tooth movement process, are Osteoclast and Osteoblast [7]. Osteoclasts are triggered to absorb the bone on the compression area and osteoblasts are triggered to generate new bone on the tension area. The processes are called bone modeling and bone remodeling, respectively [8,9]. These two processes result in tooth

movement. A theory states that compression in PDL will trigger the osteoblasts to generate some precursor molecules which stimulate the osteoclast release, while PDL tension stimulates the production of osteoblast precursor molecule, increases the osteoblasts activity, and deposits new bone [10]. As a conclusion, orthodontic loading generates tooth movement by generating compression in the PDL in the direction of movement and resorbing bone, while also generating tension in the opposite direction to create new bone.

The orthodontic load determines the stresses in the PDL and bone. Lower stress in PDL may not produce sufficient tooth movement effectively while excessive higher stress(exceeding certain threshold) may result in unwanted side effects, such as pain and excessive necrosis (dead bone) to prolong the treatment [11]. In a previous study, researchers found out a phenomenon that blood transportation in PDL capillary vessels would be blocked if the stress in PDL reaches to 8-10 KPa [12,13] and the lack of blood supplies may cause bone necrosis or even tooth damage and diseases. Root resorption/damage/bone necrosis and excessive pain are unwanted side effects due to excessive stress in PDL [12,13]. It is very critical to understand the correlation between the stress caused by orthodontic loads and biological effects affecting the tooth movement in order to optimize the orthodontic treatments.

The mechanical load impacts the tooth movement and movement pattern. The resulting stress affects the cell responses and the force and moment in the load system determine how teeth move. The reason behind the phenomenon can be explained by the concept of the tooth's center of resistance (CRes). CRes is a hypothetical point in the tooth. Figure 1.2 shows that a pure translation occurs if the resultant force passes through the CRes. Otherwise, tipping or rotation will occur due to the moments generated by the force about the center. Thus, the location of CRes is critical for determining the combination of the force and moment to control the tooth movement, such as tipping, translation, or their combination.

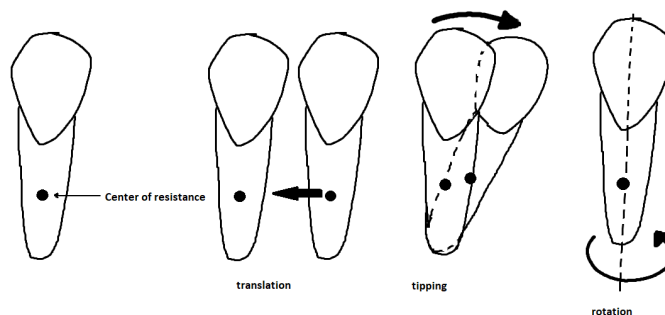


Fig. 1.2.: Tooth anatomic structure

### 1.3 Finite Element Method and Cone-beam Computed Tomography

The mechanical environment (ME) is defined by the state of stress and strain. ME in a tooth and its surrounding tissues changes when an orthodontic force is applied to it. It is not practical to measure the ME changes clinically. Therefore, analytical methods are essential. Finite element method (FEM) has been used to analyze displacement, stress and strain in biological tissues [14, 15]. The method requires modeling the biological structure using the information of the structure, geometry, and material properties of the tissues and computes the stresses, strains, and initial displacements virtually through applying proper boundary conditions. The structure and geometry can be obtained by 3D images and the material properties can be obtained experimentally, which have been investigated heavily in previous studies [16, 17].

Cone Beam Computed Tomography (CBCT) technology is commonly used for creating 3D images for dental uses [18]. It uses a lower dose of radiation than medical CT, thus can be used multiple times to record biological changes during the treatment. The technology also provides the information needed for FEM. The tissue geometry can be extracted from the images, and the morphological change can be quantified from the sequence of the images. The geometry can be used to build the FE model and the biological changes can be related to the mechanical environment changes determined using the FEM. The method has been used to validate theories relating

treatment to the clinical outcomes [15,19–21]. The challenge is to build up a reliable FE model with optimized element parameters and analysis settings to get accurate results in the shortest time.

### 1.3.1 CBCT Limitations

There are limitations in CBCT technology that can reduce the accuracy of the results. The resolution is relatively low compared to medical CT so that tissues that have the size less than the resolution, such as PDL, will not be detected in the image. Motion blur caused by head movement due to breath or other disturbance affects the clearness of the tissue boundaries, causing errors. Efforts have been made in the previous studies to stabilize the head during the scanning. Different machines and settings may also result in different image qualities and results. For longitudinal studies, the scans should be performed on the same machine with the identical settings. These limitations should be aware and assessed when the images are used.

## 1.4 Initial Displacement and Stress

Initial displacement and stress of teeth obtained from FEM had been used to predict the outcome of orthodontic treatment. Previous studies had shown that the initial displacement is correlated with the tooth movement [10,22–24].

The orthodontic loads on teeth generate the stress and strain in PDL. It is commonly accepted that the stress and strain affect differentiations in different cells which increase the activities of osteoblasts and osteoclasts. Osteoclasts absorb existing bone on the compression side and osteoblasts formulate new bone on the tension side. A tooth moves by resorbing bone in the direction of movement and generating new bone in the opposite direction which can be referred to bone modeling and remodeling [25,26]. In fact, the modeling process and remodeling process are dynamic processes that have not been fully clinically investigated yet. Multiple factors are in-

volved during this process, which are not clear at present. Therefore, the final tooth movement is not readily predictable.

Furthermore, previous studies on a mechanical environment used finite element method to calculate the initial response in teeth, PDL and alveolar bone [15]. The geometrical information was usually taken by CBCT prior to when treatment had begun. Therefore only the initial outcomes could be derived.

Besides the initial displacement, the pattern of stress field in the root and PDL, contact status, and sliding distance between wire and brackets are worth examining as well. The information is very useful in understanding the cell activities because these are stimulating factors and outcomes. According to the stress distribution pattern and displacement results, researchers can analyze the stimulation level that the cells sense and whether the target teeth are undergoing tipping, translation, rotation, or combinations initially.

Boundary condition is critical for the accuracy of a FE model. It consists of constraints at the interfaces. Wires can slide in the slots of bracket in sliding mechanics. The archwire serves as a guide. Teeth slide on the wire through brackets so that the final location can be controlled by the wire. There is a clearance between the bracket slot and the wire. When a load is applied to a tooth, the tooth has an initial displacement. Due to the low elastic behavior of the PDL, the crown has the tendency to have a relatively large displacement, which changes the contact condition of the wire and bracket. The sliding between the wire and bracket, the interaction between the wire and bracket, and the contact between the root and bone affect the load on the tooth, which triggers the tooth movement. Therefore, for sliding mechanics, the ability to model the load system including the bone, PDL, tooth, bracket, and wire in a more realistic way is needed.

The load system on the tooth is critical to control tooth movement and understand the associated mechanism. The resulting mechanical environment change triggers cell activities in PDL and bone, leading to bone modeling and remodeling. The load is delivered through activation of the orthodontic appliances, such as segmental wire,

coil spring, etc., and is the resultant of combined load from the arch wire, actuators, and frictions. Researches have been done to quantify the load on teeth. Previous experimental and computational studies [27–29] have been ignoring the sliding effects between the wire and brackets, the crowns, which may have major effects on the results. The effects need to be quantified.

It is expected that the tooth will move in the direction of orthodontic load. However, in fact, the final tooth movement is of interest, which depends on biological reactions happening in the region. It is still critical to understand the initial mechanical environment changes, which leads to reactions of the cells and subsequent biological changes. The knowledge will help predict the final tooth movements.

### 1.5 Space Closure in Orthodontic Treatment

Space closure is a process with challenge and difficulty in orthodontic treatment. It is used to correct malocclusion and fills the space due to extractions. Prescribed load system should be applied to the teeth in order to move the teeth quickly in a well-controlled way so that side effects will be minimized. Due to the difference in severity and physical condition, personalized treatment methods are needed. These require knowledge of the load system corresponding to different treatment methods. There are two prevalent clinical techniques, canine retraction and en-masse retraction, involved in space-closure. The canine retraction is done first followed by en-masse retraction of the incisors [27, 30, 31]. Segmental wire has been commonly used for canine retraction.

Custom-made wires with loops (Figure 1.3) have been made to move the tooth. T-Loop is commonly used, which is anchored on the molars and acts on the canine. The treatment strategy is implemented by adjusting the moment-to-force ratio delivered to the canine.



Fig. 1.3.: Custom-made segmental wire with T loop

The en-masse retraction of all the incisors is used after the retraction of the canine. But in some cases, the canine is also bonded together with the incisors. The goal is to retract the entire incisors (and canineto) to fill the space that occurs after the canine retraction1st premolar extraction. The teeth are aligned first. The incisors (and canine) are bounded. A stiff wire is going through the slots of the brackets, which are aligned. Power arms are attached to the bracket on the canine or the portion of the stiff wire between the canine and lateral incisor. The retraction force is provided by coil spring, which is hooked to the end of the power arm and an implant - miniscrew. (Figure1.4) In this case, the anterior teeth are pulled in distal direction by the orthodontic load from the coil spring. The stiff wire serves like a guiding wire such that the teeth can slide on it. The system is called sliding mechanics. It is important to understand the load systems that different appliances can deliver to the targeted tooth to better control its movement.

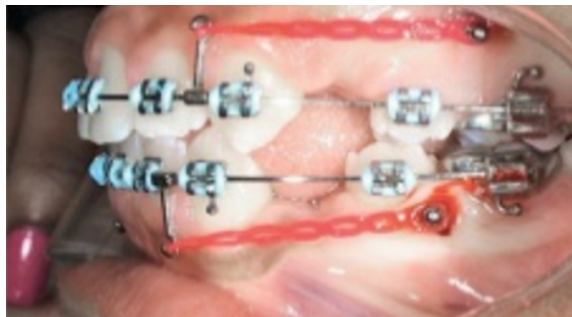


Fig. 1.4.: Power arm and implant in en-mass retraction

## 1.6 Knowledge Gap

### 1.6.1 Previous Relevant Work

Over the past few decades, orthodontists and other researchers had been trying to predict clinical outcomes such as final tooth movement as well as the stress and strain that affect tooth movement during the orthodontic treatment period. In the early studies, researchers had to simplify the system by idealizing factors in order to make the problem solvable due to lack of high performance computers and effective software [32]. FEM has been used in orthodontic research. It can be used to determine the mechanical environment changes in complex system with irregular geometry and boundary conditions. Although the tooth and the surrounding tissues complex, FE models are getting more and more realistic and complex to improve the accuracy. Mice and human FE models are created from CT scans and were used to predict the outcome of clinical treatments [21, 29, 30]. Because the models were simplified differently, the results in terms of location of CRes, stress distributions and magnitudes, etc. have discrepancies [33–36]. The following figures show some simplified models that were used for canine retraction (T-Loop) case and en-masse retraction case from previous researches. Figure 1.5 shows the model used for the canine retraction (T-Loop) case. The model in the figure is a single canine model which only contains canine and no other surrounding teeth [37]. With this model, we cannot determine whether the surrounding teeth could affect the canine or not.

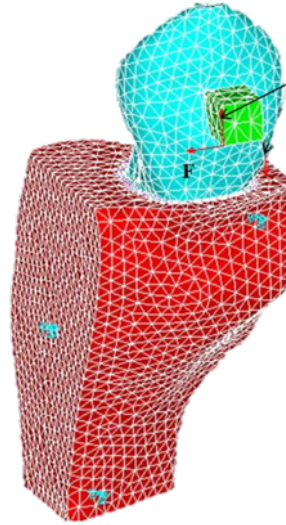


Fig. 1.5.: Previous model for canine retraction with T-Loop [38]

Figure 1.6 shows the en-masse retraction models in the previous studies. In the first model [39], all the teeth were bonded together by the connection in geometry. This simplification turns all the teeth into one part which changes the movement pattern of teeth. In the second model [28], the wire is bonded to the brackets. Because this is sliding mechanics, friction or binding will occur in an en-masse retraction case. Thus, this bonded simplification may not be realistic.

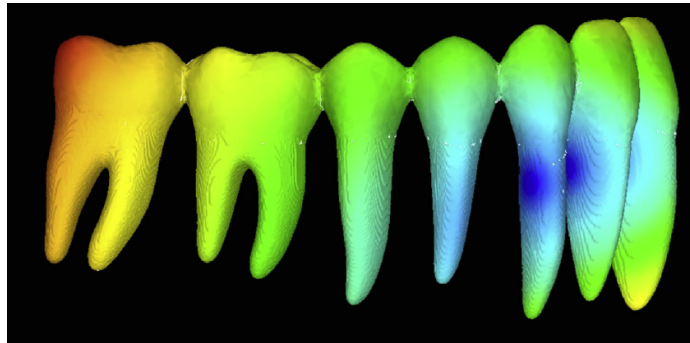


Fig. 1.6.: Previous model for en-masse retraction case

Figure 1.7 shows the location of power arm in the en-masse retraction case from a previous study [40]. In this study, the power arm was only put on the wire with a different location. But in clinical studies, the power arm could be put on the bracket. Thus, due to the locations of the power arm, the differences of effect in ME are not clear.

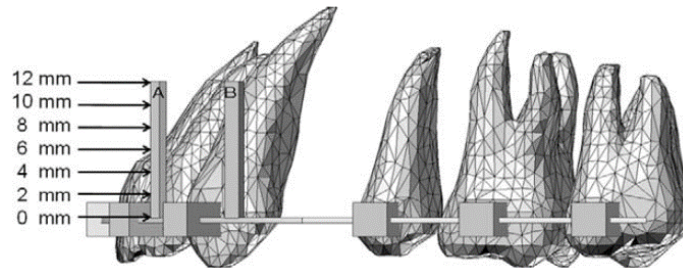


Fig. 1.7.: Previous model for en-masse retraction case

### 1.6.2 Types of Boundary Conditions

Previous studies have models of a single tooth or multiple teeth. Typically, there are two types of boundary conditions, contact and bonded (frictionless) for different clinical cases. A single tooth model may be good for a frictionless system, like segmental wire, because the load is applied only to a single tooth. A multiple teeth model should be considered when sliding mechanics is analyzed because the interaction among the neighboring teeth needs to be included. When multiple teeth are involved for a sliding mechanics application, the boundary conditions are complex because the relative motions between the teeth, the bracket and wire, and ligations need to be simulated correctly.

Several clinical treatments, canine retraction and en-masse front section retraction, need load information on the teeth to be moved to control the displacement patterns, tipping/translation. The commonly used appliances are segmental loops and sliding mechanics [27, 31]. Segmental loop has been used for canine retraction and is frictionless while the sliding mechanics has been used for en-masse retrac-

tion [40]. The segmental loop is commonly used for moving a single tooth. Sliding mechanics has been used for en-masse retraction, which involved multiple teeth. The sliding mechanics consists of multiple brackets, a guiding wire, and actuator, typically coil spring or elastomer. [Figure 1.4] Brackets are attached to the crowns and wires are put into the slots of brackets. The actuators are attached to the moving segment, which are anchored through a distal segment or an implant. When multiple teeth are involved, the correct boundary conditions require relative motion between teeth and bracket-wire interfaces.

FE models have been developed to analyze a load system on the teeth. Most models have been simplified and have not provided the information clinicians need. Even in canine retraction case, no study before modeled the surrounding teeth to see if the canine retraction affects other teeth other than the canine itself or how much the influence is, although clinical evidence shows some effects. In the en-masse retraction case, rigid wire was modeled with much simplified boundary conditions, such as binding the interfaces that have relative motion together. It is critical to evaluate the effects of the simplification on the outcomes so that the validity of previous studies can be estimated.

## 1.7 Research Objectives

The overall goal of this research is to be able to obtain a more accurate load system on teeth. The objectives are: 1) to build up a reliable model with details that can be more reliably utilized to simulate different orthodontic clinical cases, which will help orthodontists to predict the treatment outcomes, 2) to assess the significance of the differences between the simplified model and the models with more details, and (3) to apply the technology to clinical cases and estimate ME changes.

## 2. MATERIALS AND METHODOLOGY

### 2.1 Overview

An entire mandible was used for this study and the mandible was scanned using cone-beam CT (I-CAT machine). Due to symmetry, only half of the mandible was built. The volunteers second and third molar on the right had been extracted. The FE model was built by three steps: the dental structure segmentation from the CBCT by using MIMICS 16 (Materialise, Belgium); geometry rebuilding in CReo Parametric 2.0 (PTC, Massachusetts); and the FE modeling in ANSYS workbench 17.1 (ANSYS, Pennsylvania). Three clinical cases were simulated with this model. The tooth movement pattern and stress in PDL was analyzed and compared.

### 2.2 Material

A CBCT scan of the mandible from an adult anonymous patient was used. The scan can be viewed in XY, YZ, XZ planes in MIMICS which are called transverse plane, sagittal plane and vertical plane respectively. The pixel size of the scan is  $0.25 \times 0.25 \times 0.25 \text{mm}^3$ .

### 2.3 Geometry Reconstruction

#### 2.3.1 3D Segmentation of the CBCT Scan

The CBCT images were imported into MIMICS to construct the 3D teeth (incisor, lateral incisor, canine, 1st premolar, 2nd premolar and 1st molar) and alveolar bone. The occlusal plane was aligned with the XY plane (horizontal plane) as shown in Figure 2.1. Each voxel has a size in the CT scan as 0.25 mm, with a grey scale value

associated. The grey scale value represents the calcification level of the tissue. Thus the dense bone has higher grey scale value.

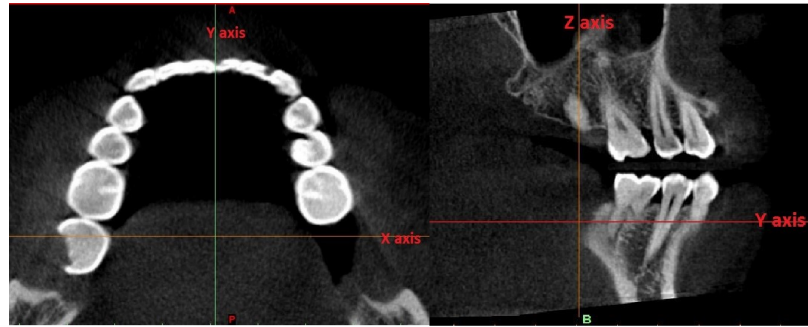


Fig. 2.1.: X, Y, Z axis in Mimics

All the six teeth were semi-automatically segmented by setting a threshold range of the grey scale value and then manually clearing the defects. As the grey scale value may have regional changes in CBCT, an individual threshold, which best isolates the root from the environment, was set to each tooth for segmentation. Due to the motion blur, automatic segmentation cannot perfectly isolate the tooth. Manual operations were applied to clear the defects. The neighbor alveolar bone was segmented similarly for further FE modeling purpose. The motion blur can reduce accuracy of scans which is caused by the vibration of the patient that occurred during the radiation process. The motion blur and the low resolution lead to the failure to isolate the PDL and cortical bone around the tooth. In this study, the PDL and surrounding cortical bone were grown from the root surface, which is introduced in the following section.

Polylines were created after segmentation. Polylines represented the boundary of the structure and were used to rebuild the geometry in CREO. To efficiently build the model, not all the polylines were used. Only critical and necessary polylines were selected and exported to CREO. See Figure 2.2 for polylines and selected polylines.

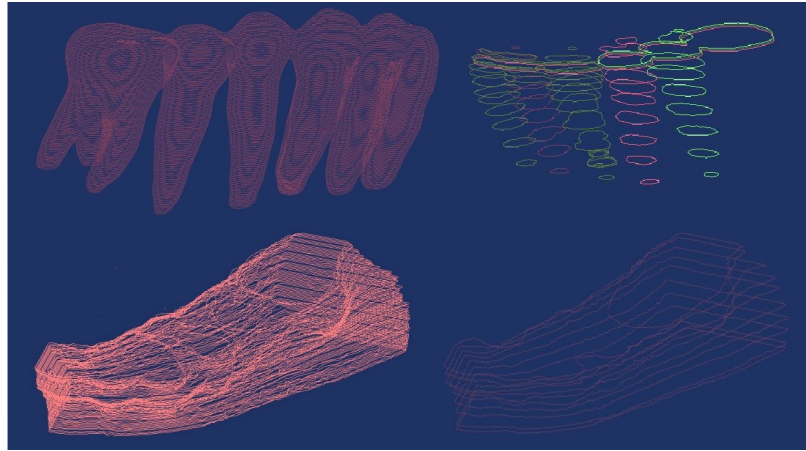


Fig. 2.2.: Teeth polylines(upperleft),alveolar bone polylines(lower left), selected teeth polylines(upper right),and selected alveolar bone polylines(lower right)

### 2.3.2 Reconstruction of the Tooth, PDL and Cortical Bone

Teeth and alveolar bone were reconstructed in CREO based on their polylines built in MIMICS. Each polyline was duplicated and smoothed by the spline function. (See in Figure 2.3) Then the feature swept blend was conducted with these splines to reconstruct the final geometries. For each tooth, the crown and root were built in separate swept blend (Figure 2.4).

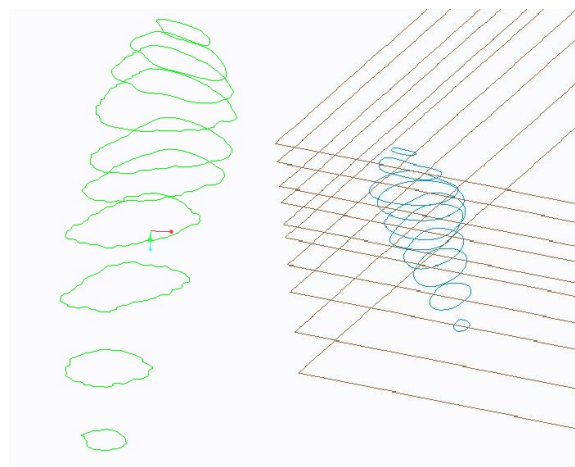


Fig. 2.3.: Polylines in Creo (left); Sketch planes and spline lines (right)

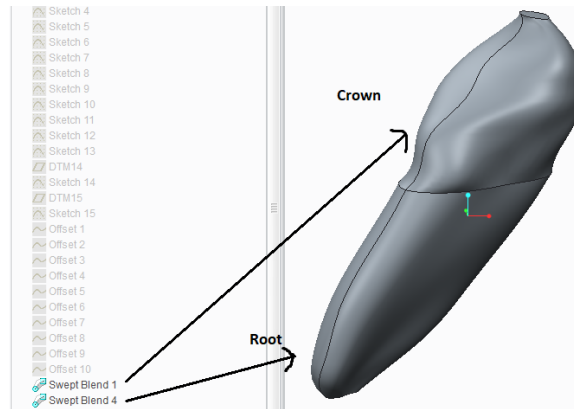


Fig. 2.4.: Final geometry of canine. It was consist of crown and root.

The PDL and surrounding cortical bone were built by offsetting the surface of the root with 0.2 mm. As mentioned previously, the PDL and cortical bone cannot be distinguished in CT scans so that a reconstruction process needs to be employed in CREO. In the modeling process, we assumed the PDL and cortical bone is uniform in thickness of 0.2mm[7]. Based on the splines of the root that had been generated previously, a 0.2mm offset value was applied radially to each spline of the root to form the boundary of the PDL and another 0.2mm offset value for the cortical bone. There is an additional 0.2mm offset in the vertical direction on the bottom layer of spline which makes the PDL and cortical bone completely cover the root and PDL respectively. (See Figure 2.5) The PDL and surrounding cortical bone were then reconstructed by using the Swept Blend function. As the root and crown were constructed separately in the previous step, the crown would not affect the geometry of the root. Then the thickness of the PDL would be homogeneous. Each structure was saved as sat files and exported to ANSYS Workbench.

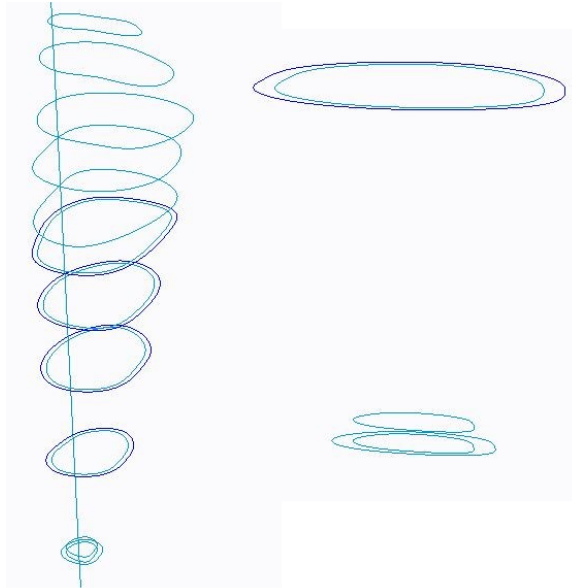


Fig. 2.5.: 0.2mm offset spline line was set to generate PDL horizontally and vertically

The orthodontic wire and simplified brackets were also built in CREO based on their actual size used in clinics. The slot size of the bracket is 0.022-in and the stainless steel arch wire is  $0.016 \times 0.022$ -in (See Figure 2.6) .The unnecessary details of the bracket were not modeled.

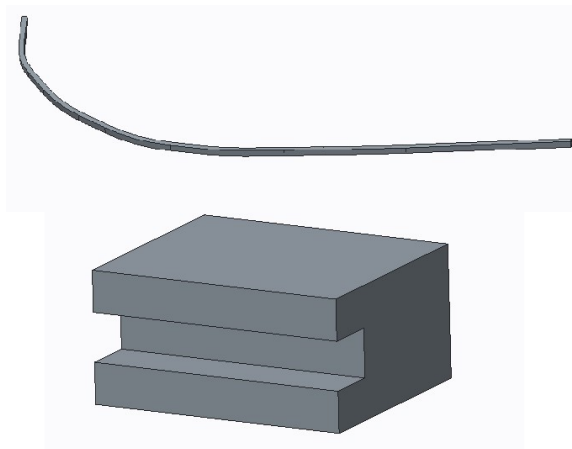


Fig. 2.6.: Orthodontic wire and simplified bracket

## 2.4 Finite Element Modeling

### 2.4.1 Geometry Assembly

SAT files were input into the geometry section of ANSYS Workbench and were regenerated into solid models. Boolean operations were performed to assemble the model. The shape of the cortical bone and PDL are like shells and the bone covers the PDL while the PDL covers the root(Figure 2.7). We used the Boolean operation to create the geometry of PDLs, cortical bones, alveolar bone, and brackets. The particular operations are: subtract and unite.

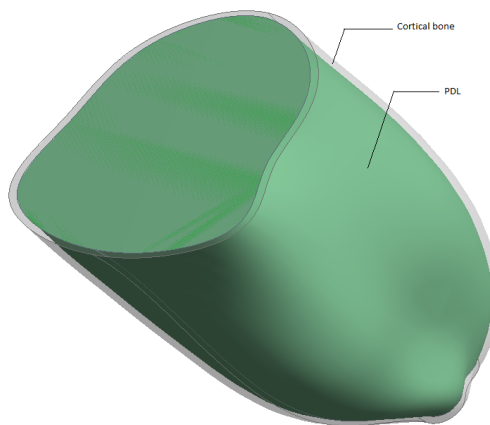


Fig. 2.7.: PDL (green, covered by bone) and cortical bone (transparent layer)

The finite element model consisted of the archwire, brackets, tooth, PDL, cortical bone and alveolar bone. The schematic (vertical sectional view) of the model is shown below in Figure 2.8. The locations of the brackets and wire were based on a typical clinical treatment.

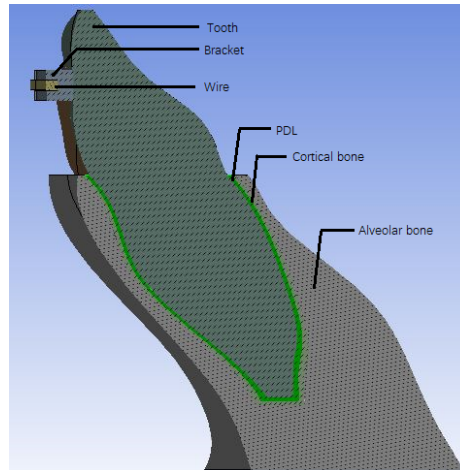


Fig. 2.8.: Vertical sectional view of the model

#### 2.4.2 Material Properties

The tooth and cortical bone are dense material while the alveolar bone, which is mainly cancellous bone, has relatively lower density. The PDL is considered to have uniform thickness. The material properties of the model are shown in TABLE 2.1 below.

Table 2.1.: Material Properties

	Young's Modulus	Poisson Ratio	Reference#
Tooth	20,000 MPa	0.3	44
PDL	0.47 MPa	0.45	7
Cortical bone	10,000 MPa	0.3	44
Cancellous bone	2,100 MPa	0.3	44
Arch wire	193,000 MPa	0.31	ANSYS database
Bracket	193,000 MPa	0.31	ANSYS database

The teeth, PDL and alveolar bone used in the model were assumed to have isotropic and homogeneous linear elasticity. The Young's modulus and Poisson's ratio in this study were set as same as those in the previous literatures [7, 41].

## 2.5 Boundary Conditions

Figure 2.9 shows the model that consisted of central and lateral incisors, canine, 2nd premolar, alveolar bone, brackets and wire. For simulating the Power Arm case, an implant (miniscrew) should be used to provide anchorage of a coil spring that applies an orthodontic force to the power arm. The force was known thus the implant was not modeled. There were multiple interfaces. Some interfaces did not allow relative motions, such as the interfaces between bracket and tooth, PDL and bone, PDL and root, which were bonded. The interfaces that allowed relative motion included the interfaces between the crowns and some of the interfaces between the brackets and archwire. For comparison purpose, these interfaces (allowed relative motion) were either bounded for the simplified models, which have been used in previous studies, or modeled using contact elements, which allow relative motion. The ligation was modeled, which will be discussed later.

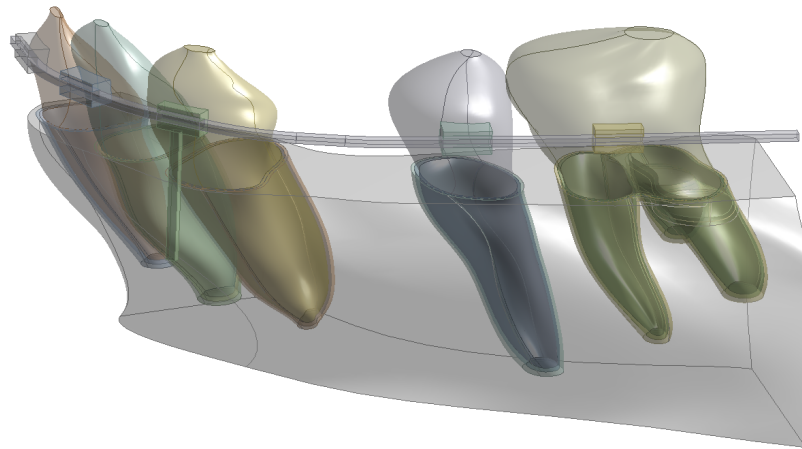


Fig. 2.9.: Final model overlook (for canine power arm case and en-masse retraction case)

Only half of the mandible was modeled due to symmetry. The constraints (boundary condition) of the half mandible model are shown in Figure 2.10. The model had two surfaces constrained, one at the central sagittal plane, and the other one at the distal surface behind the molar. The mandible acts like a cantilever. The posterior surface, A, was fully constrained. The anterior surface, D, was constrained only in the direction perpendicular to the surface, which represented the symmetry. For the T-loop case, there was no archwire. The fixed support at the surface A and the symmetry constraint at surface D were the same for all the models.

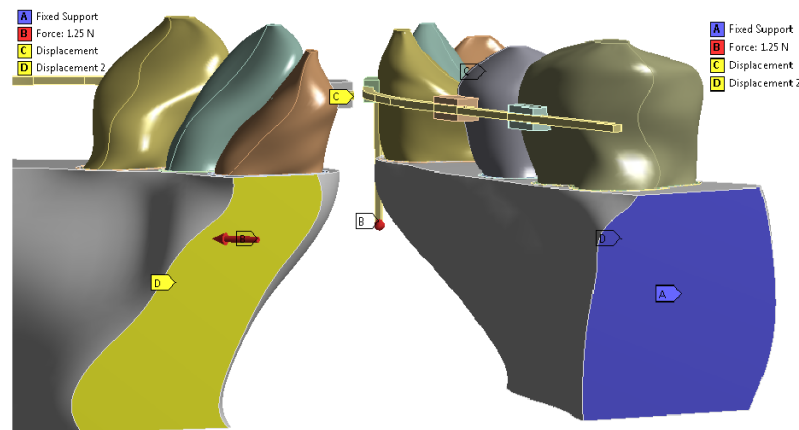


Fig. 2.10.: The boundary conditions of the half mandible model. (Tag C and D in yellow are displacement constrain and Tag A in blue is fixed constrain. Tag B in red is the applied force)

The interfaces between the brackets and the archwire have relative movement. They were typically fixed in the previous studies, but will be modeled using contact elements in this study. Both were modeled in this study for comparison purpose. Figure 2.11 shows two different contact types between the wire and the brackets.

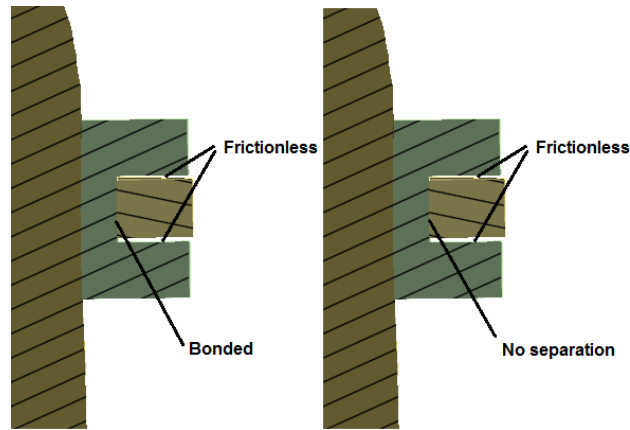


Fig. 2.11.: Two contact types between wire and brackets

Totally, five models were built. The purpose of each model is described below. The specifics of each model is shown in Table 2.2

Table 2.2.: Model Descriptions

Model#	Treatment	Contact	Purpose
1	Segmental T-Loop	Yes	OBJ #1 and OBJ #3
2	En-masse (Power arm on canine)	Yes	OBJ #1 and OBJ #3
3	En-masse (flexible wire)	Yes	OBJ #1 and OBJ #2
4	En-masse (rigid wire)	Yes	OBJ #1 and OBJ #2
5	En-masse (power arm on wire)	Yes	OBJ #1 and OBJ #3

### 2.5.1 1<sup>st</sup> Model Set Up (Canine Retraction with Segmental T-Loop)

The purpose of this model was to find out the changes of ME in PDL and bone of the segmental T loop case, to find out the displacement of canine, to check whether it is worthy to model adjacent teeth, and to perform a convergence test. The archwire and 4 brackets were omitted in this model because the segmental wire was mounted between the posterior segment and the canine, and the archwire was not applied.

The element size need to be determined based on the result of convergence test which are described at the end of this chapter. (Section 2.6) The contact element size of canine was set to 0.6mm for alveolar bone, cortical bone, PDL and root. The reason to use contact sizing rather than global element size was that the elements number of the model can be controlled in a relatively low scale which could save numerous analyzing time and computational resources. If the element size was applied to all the parts in this model, it might take days to finish the analysis. The number of elements in this model was 111,061 and the number of nodes was 208,238. Figure 2.12 shows the meshing details of this model.

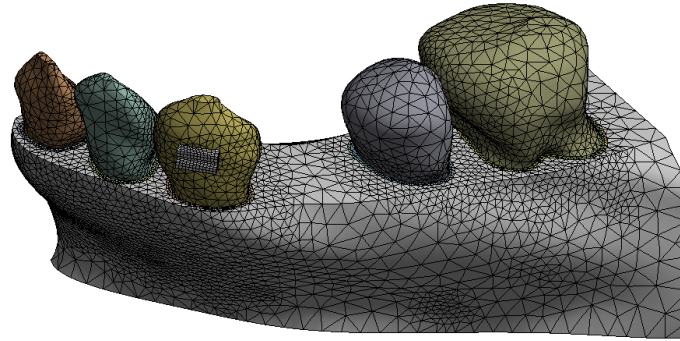


Fig. 2.12.: Meshing overlook of canine (T loop) model

The loading condition is shown in Figure 2.13. The orthodontic loads included one horizontal force B (1.25N) and two correctional moments that were generated by two couples of force(C,D and E,F). The direction and value of the forces were calculated based on the CRes of canine. The CRes of tooth is at 60% height of root (from apex to alveolar crest)[40]. The forces C and D were one couple of forces with the value of 3.46N and one towards to root while the other towards to crown. They cancelled the moment caused by horizontal force B about the CRes in order to prevent canine from tipping in distal direction. The forces E and F were another couple of force with the value of 3.63N in buccal lingual direction. They cancelled the moment caused by force B to prevent canine from rotating about its long axis. Ideally, this orthodontic

load would lead to a translation movement to canine. There were one displacement constraint and one fixed constraint on the alveolar bones as described before.

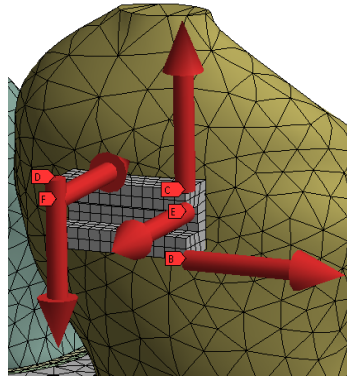


Fig. 2.13.: Equivalent forces of T loop that were applied on bracket in canine T-Loop model

### 2.5.2 2<sup>nd</sup> Model Set Up (Canine Retraction with Power Arm)

The purpose of this model was to compare the mechanical environment changes caused by two different orthodontic appliances and check the effect on tooth, PDL and the bone. This model corresponded to the clinical case of canine retraction using the bracket with a power arm. The teeth, PDLs, cortical bones, alveolar bone, brackets, archwire, and power arm (on the canine bracket) were modelled. The location of the implant determined the direction of the orthodontic force, and modelling the geometry of the implant was not necessary. Figure 2.14 shows the meshing details of this model. The model had 204,516 elements and 345,865 nodes.

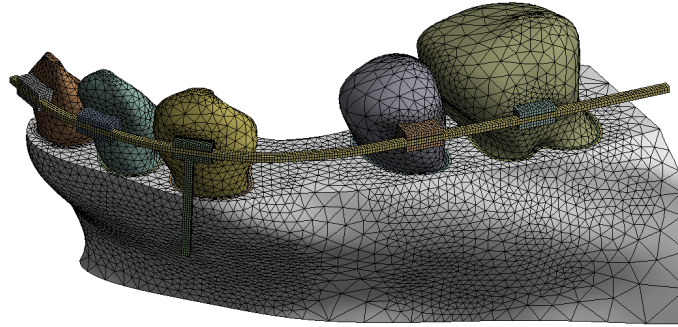


Fig. 2.14.: Meshing overlook of canine retraction (power arm) model

Figure 2.15 shows that a 1.25N orthodontic load was applied on the end of power arm towards the implant which was between the 2nd premolar and 1st molar. This single force represented the force from the coil spring that connected the power arm and implant. The wire was bonded to the brackets of the two incisors and could slide (no separation) in other brackets. In order to achieve canine translation movement, the orthodontic force should be applied right through the Cres, and length of the power arm was 8.323mm downward from the bottom of bracket. The length was calculated by the 60% length (from apex to alveolar crest) of the root[40]. There were two displacement constraints (they are on the wire and alveolar bone and perform the symmetry function) and one fixed constraint in this model as described before.

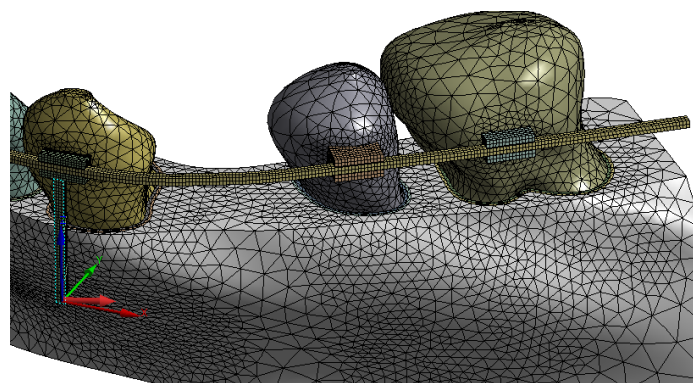


Fig. 2.15.: Loading condition (Horizontal force in XY plane towards to implant)

### 2.5.3 3<sup>rd</sup> Model Set Up (En-masse Retraction with Flexible Wire)

The purpose of this model was to find out the changes of the mechanical environment in PDL and to predict the clinical outcomes. This model corresponded to the clinical case of en-masse retraction with sliding mechanics. The en-masse retraction model was pretty similar to the power arm canine retraction model. Instead of that the wire was bonded to two incisor brackets in the 2nd case, the wire was bonded to three brackets, including the canine bracket. Only two slots were set to no separation in this model which were the 2nd premolar and 1st molar brackets.

According to the previous studies, 100cN to 300cN orthodontic loads were found in the previous models. In order to compare the results, the load was set to 125cN as well. The other parameters remained the same. Figure 2.16 shows the meshing details and loading condition.

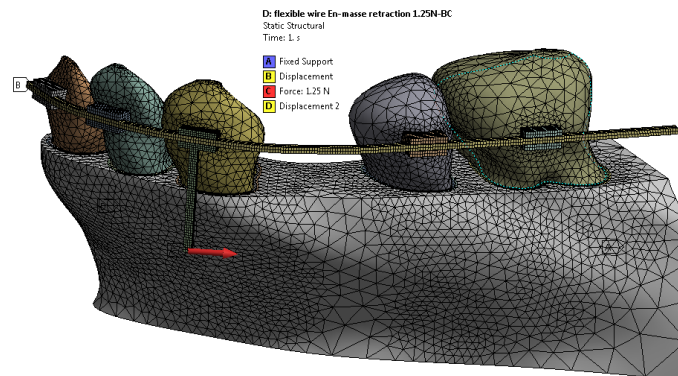


Fig. 2.16.: Meshing overlook and loading condition of en-masse retraction (flexible wire) model

### 2.5.4 4<sup>th</sup> Model Set Up (En-masse Retraction with Rigid Wire)

The purpose of this model was to represent a simplified model from the previous study [41]. The results of mechanical environment changes in this model were compared with the previous detailed model (with flexible wire). The boundary con-

ditions and loading conditions of this model was the same as the previous model (flexible wire) except the wires stiffness behavior was changed to rigid. It means that the wire cannot deform or be meshed in this analysis. Besides, the rigid wire was bonded to all five brackets. This was to simulate the previous case that had all the crowns bounded. The meshing and loading details are shown in Figure 2.17. This model consisted of 204776 elements and 341148 nodes and a 1.25N horizontal force was applied on the end of the power arm towards the implant.

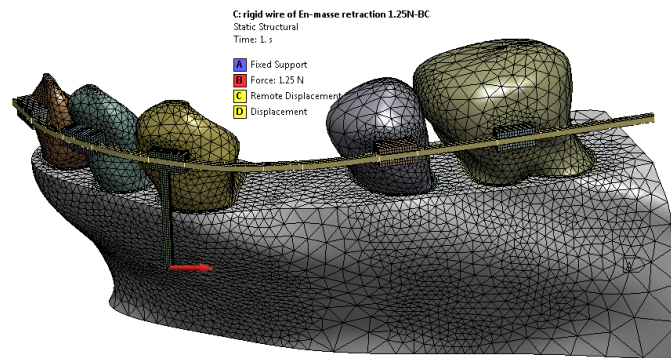


Fig. 2.17.: Meshing overlook and loading condition of en-masse retraction (rigid wire) model

### 2.5.5 5<sup>th</sup> Model Set Up (En-masse Retraction with Power Arm Attached to the Archwire)

The purpose of this model was to check the effect of a different orthodontic appliance (different location of power arm) and to compare results in the PDL and bone with the flexible wire en-masse model. In this model, the wire was remodel with the change of the power arm location (Figure 2.18).

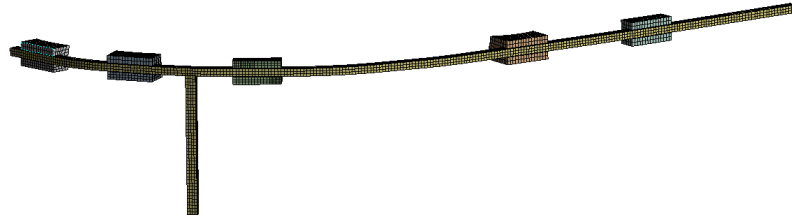


Fig. 2.18.: Remodeled wire of different cantilever location

The power arm was extruded with the orthodontic force applied to the same plane as the CRes of tooth. Except of this variation, all the settings, including the boundary conditions and loading conditions of this model, were the same as the flexible wire en-masse retraction model. This model consisted of 205,980 elements and 353,498 nodes. Figure 2.19 shows the meshing detail and the whole model.

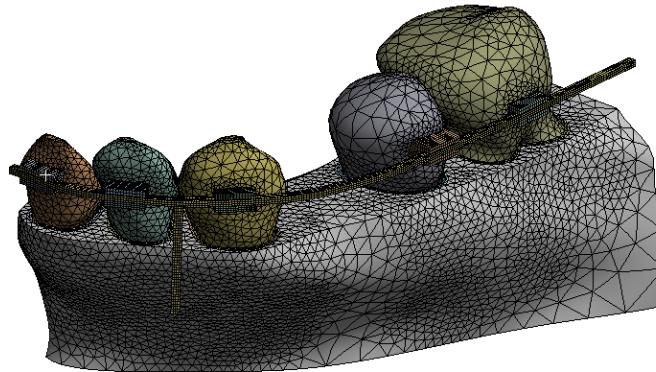


Fig. 2.19.: Meshing overlook and loading condition of en-masse retraction (power arm on wire) model

## 2.6 Convergence Test

Since the results in the finite element analysis are derived from the displacement on nodes and elements of the model, the element size/number affects the results accuracy. While the geometry of teeth, PDL and alveolar bone are irregular and nonuniform, coarse mesh size/bigger element size might not be able to provide the level of accuracy.

Thus a convergence test should be performed to decide the maximum element size for consistent and reliable results. The convergence test was conducted by gradually increasing the element number/decreasing the element size. The displacements on a same node in each analyses are evaluated. The goal is to find the maximum element size that can provide consistent nodal displacement. We have chosen 5% as the acceptable variation because this level of error does not have significant clinical effects.

The convergence test was conducted using the segmental T loop model to determine the element size. The major refinement of the elements occurred close to the contact surfaces. These elements were meshed four times with element sizes from 0.6 mm to 0.3mm with an increment of 0.1mm. With the same loading (position, direction and value), boundary conditions, and other parameter settings, the displacement at a targeted point which is the green point on the top of the crown in Figure 2.20 was calculated.

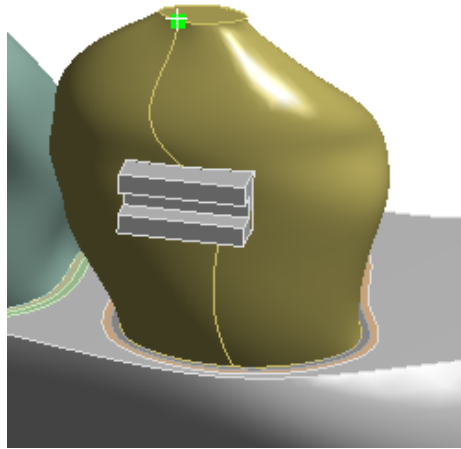


Fig. 2.20.: The chosen targeted point for displacement in the convergence test

The 3rd principal stress at a targeted point which is the green point on the PDL in Figure 2.21 was calculated. These points can be identified in all five models. The displacement and stress at the same point were recorded to check the convergence. The maximum element size/ minimum element number needed for achieving consistent results were chosen for this research.

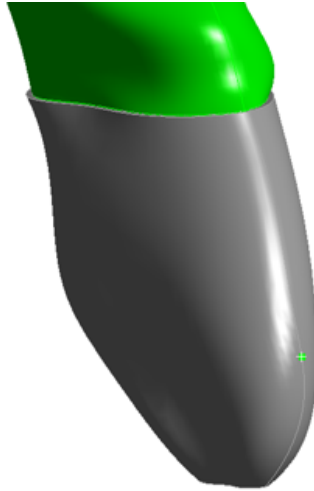


Fig. 2.21.: The chosen targeted point for 3rd principal stress in the convergence test

### 3. RESULTS

The 1st, 2nd, 3rd principal and von-Mises stresses of PDL and deformation of teeth and sliding distance of wire (if applicable) are shown in figures. The highest stress and its locations are demonstrated.

For OBJ #1, the result of convergence test had been checked using the segmental T loop model to determine the element size. For OBJ #2, the comparison of stresses from the two different en-masse retraction models were made to see whether detailed modeling is necessary. For OBJ #3, three clinically used treatments were simulated to investigate the mechanical environment changes due to the treatments.

#### 3.1 OBJ#1: To Build up a Reliable Model with Details

Table 3.1 shows the stress and displacement of the result of the convergence test based on the segmental T loop model. The results from the convergence test showed that the model with the element size of 0.6mm provides acceptable accuracy. The standard deviation of the nodal displacement was about 0.5%, and of the 3rd principal stress was about 1.9%, which have negligible effects on clinics. Thus the differences can be ignored.

Further reducing the element size would significantly increase the computing time, but would result in negligible stress difference. In the 0.6mm element size model, the computational time for the analysis was about 4 hours. And when the element size reduced to 0.2mm, it took the workstation 45 minutes to even perform the mesh. Therefore the 0.6mm contact element size was chosen to be the optimum choice.

Table 3.1.: The Results of Convergence Test

<b>1.25N</b>	<b>0.6mm</b>	<b>0.5mm</b>	<b>0.4mm</b>	<b>0.3mm</b>
Displacement	0.001407mm	0.001421mm	0.001420mm	0.001420mm
3 <sup>rd</sup> principal stress	1804.5Pa	1771Pa	1714Pa	1758Pa
Element number	109872	125196	145087	190134
Node number	219744	250392	290174	380268

Table 3.2.: Standard Deviation (STD)

	<b>Mean</b>	<b>STD</b>
Displacement	0.001419mm	6.87E-06 (0.48%)
3 <sup>rd</sup> principal stress	1758.76Pa	33.06 (1.88%)

### 3.2 OBJ #2: Comparison of the Simplified Model and Detailed Model

For the object 2, the tooth displacement, three principal stresses and von-Mises stress in PDL and cortical bone from the two En-masse retraction model were obtained. Both stress distribution and magnitude were compared. Figures 3.1 to figure 3.8 show the stress distributions from the two models. The maximum stresses in the same tissue were also shown in Tables 3.3.

#### 3.2.1 Comparison of First Principal Stress in PDL

Figure 3.1 shows the comparison of 1st principal stress in PDL from detailed model (upper) and simplified model (lower). The maximum 1st principal stress from

detailed model was 23.46KPa while the maximum 1st principal stress from simplified model was 8.15KPa.

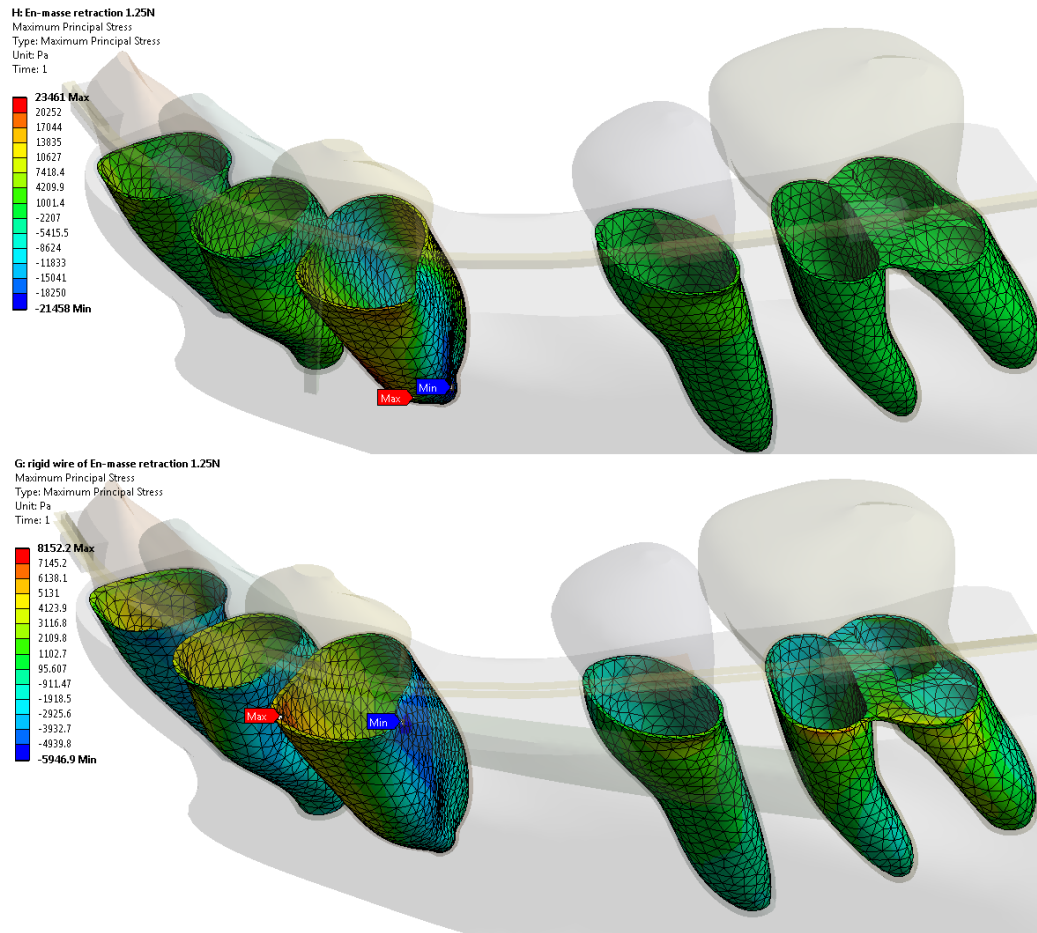


Fig. 3.1.: Comparison of first principal stress in PDL from detailed model and simplified model

### 3.2.2 Comparison of Second Principal Stress in PDL

Figure 3.2 shows the comparison of 2nd principal stress in PDL from detailed model (upper) and simplified model (lower). The maximum stress from detailed model was 16.95KPa which occurred near the bottom in PDL while the location of the maximum stress from simplified model was in the PDL of molar and the value was 6.4KPa.

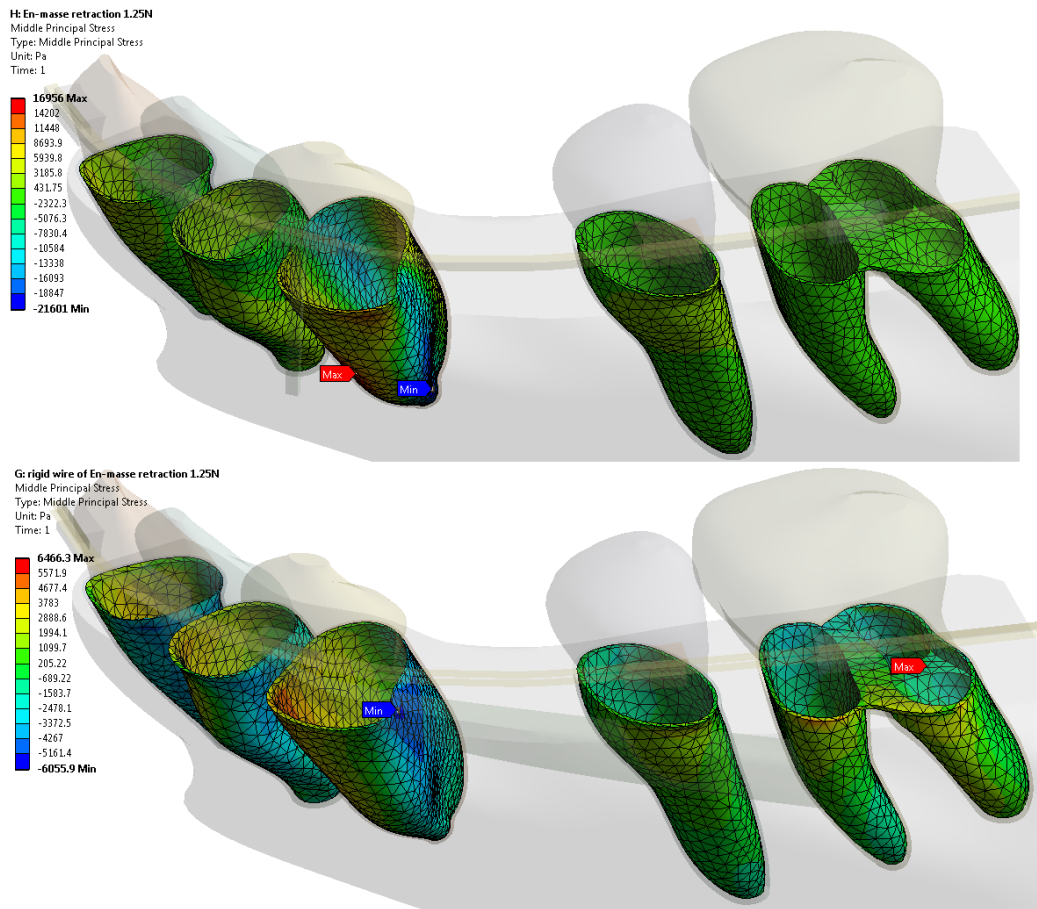


Fig. 3.2.: Comparison of second principal stress in PDL from detailed model and simplified model

### 3.2.3 Comparison of Third Principal Stress in PDL

Figure 3.3 shows the comparison of 3rd principal stress in PDL from detailed model (upper) and simplified model (lower). The maximum compressive stress occurred near the bottom in PDL from detailed model and the value was 26.9KPa. In the simplified model, the maximum compressive stress is 7.59KPa and its location was near the top of PDL. There were compressive stresses in two incisors PDL in simplified model but it was hardly to find compressive stress from the detailed model.

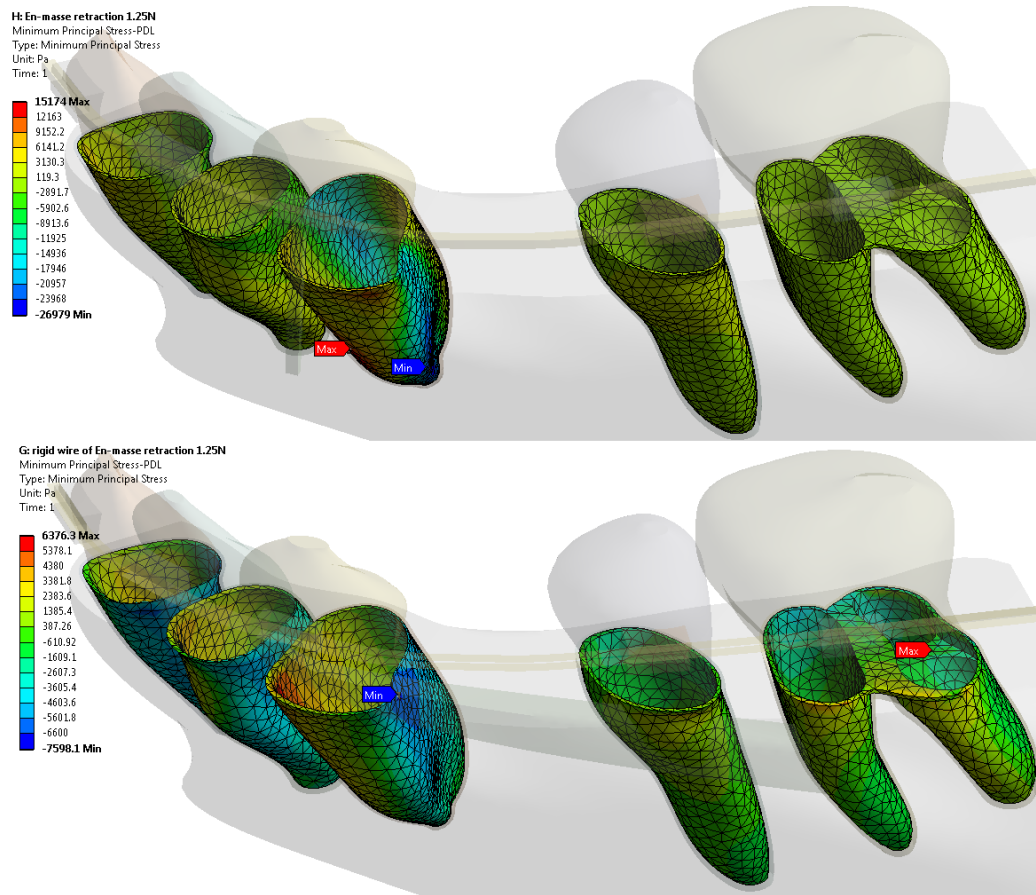


Fig. 3.3.: Comparison of third principal stress in PDL from detailed model and simplified model

### 3.2.4 Comparison of Von-Mises Stress in PDL

Figure 3.4 shows the comparison of von-Mises stress from the simplified model (upper) and the detailed model (lower). The maximum von-Mises stress 18.3KPa in the detailed model and 4.4KPa from the simplified model. The maximum stress point from the detailed model is on the inside surface of PDL and the specific location is shown in the figure. The maximum stress point in the simplified model is on the top of PDL and the specific location is shown in the figure. The simplified model had stress effect on all five PDL while the detailed model only had stress effect on the PDL of anterior teeth.

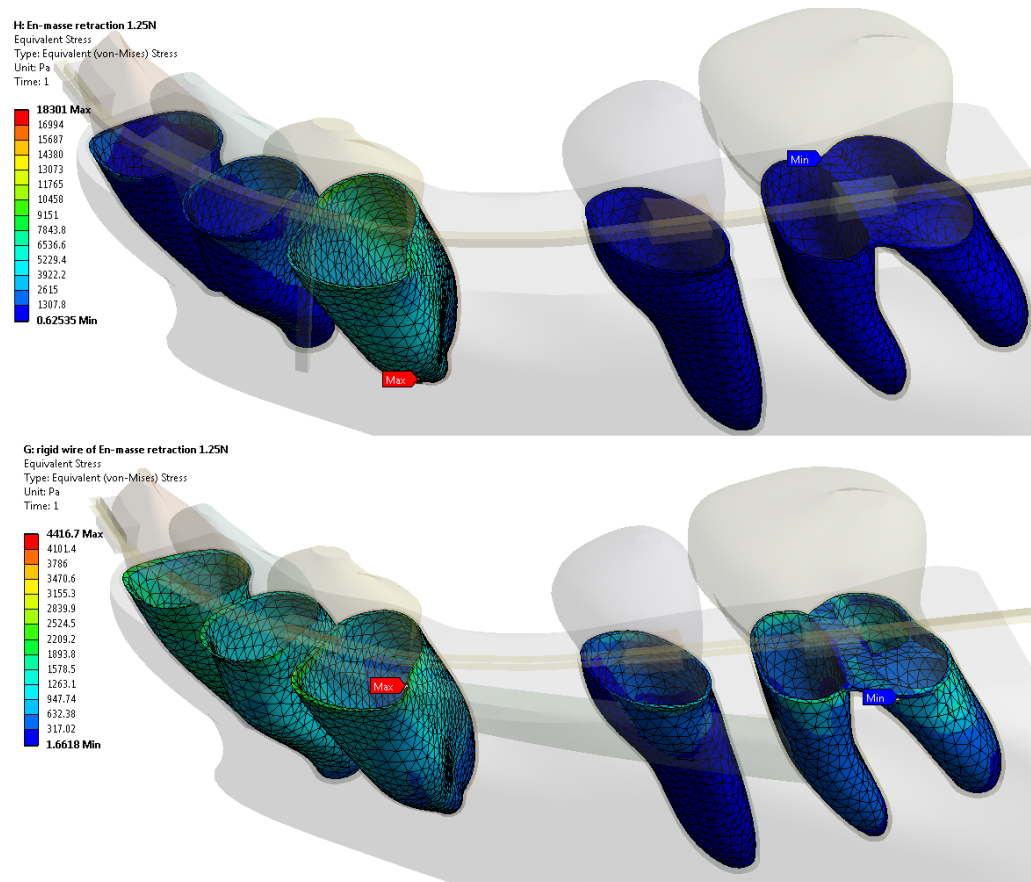


Fig. 3.4.: Comparison of von-Mises stress in PDL from detailed model and simplified model

### 3.2.5 Comparison of First Principal Stress in Cortical Bone

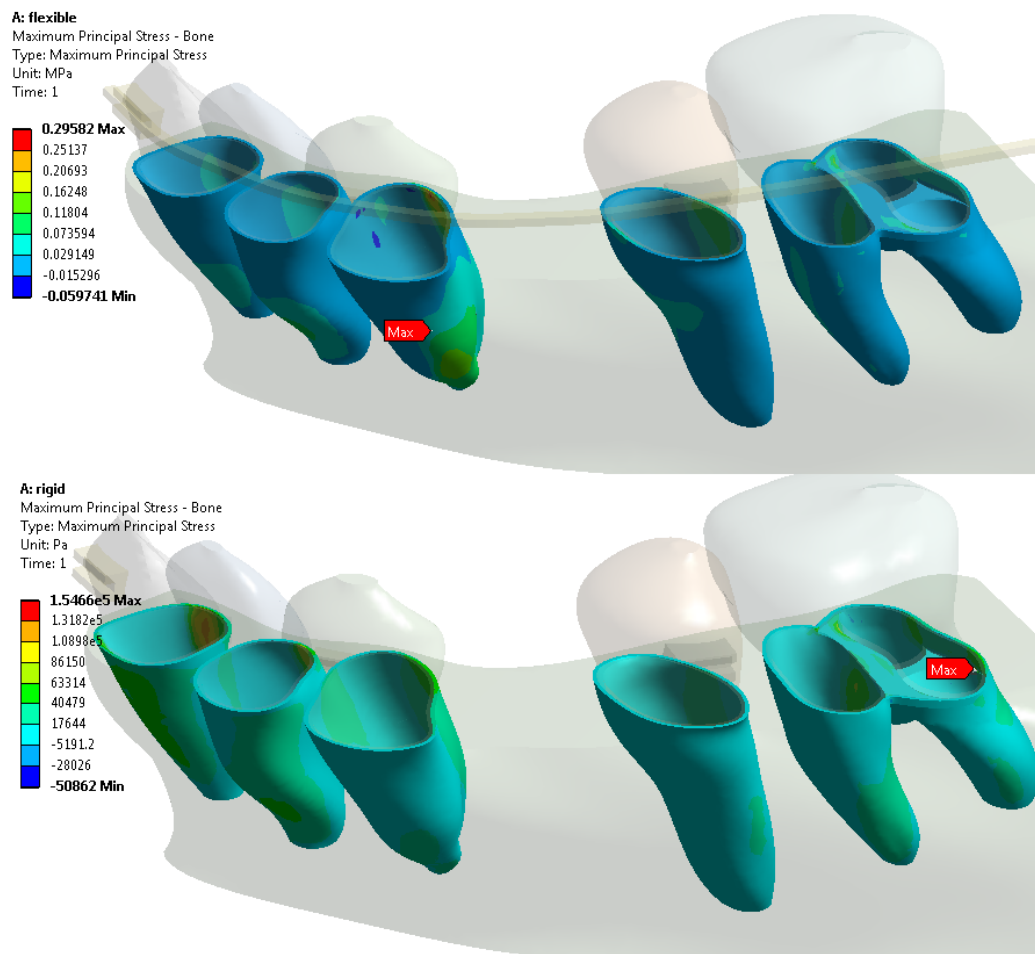


Fig. 3.5.: Comparison of first principal stress in bone from detailed model and simplified model

### 3.2.6 Comparison of Second Principal Stress in Cortical Bone

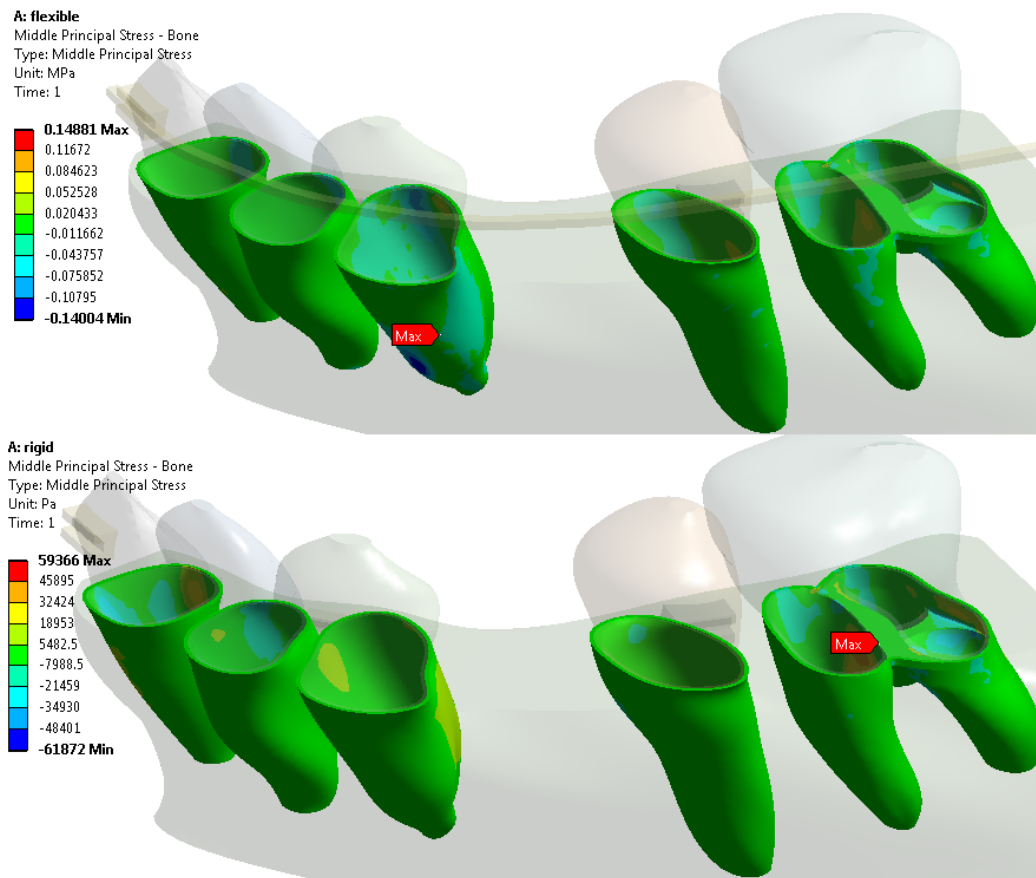


Fig. 3.6.: Comparison of second principal stress in bone from detailed model and simplified model

### 3.2.7 Comparison of Third Principal Stress in Cortical Bone

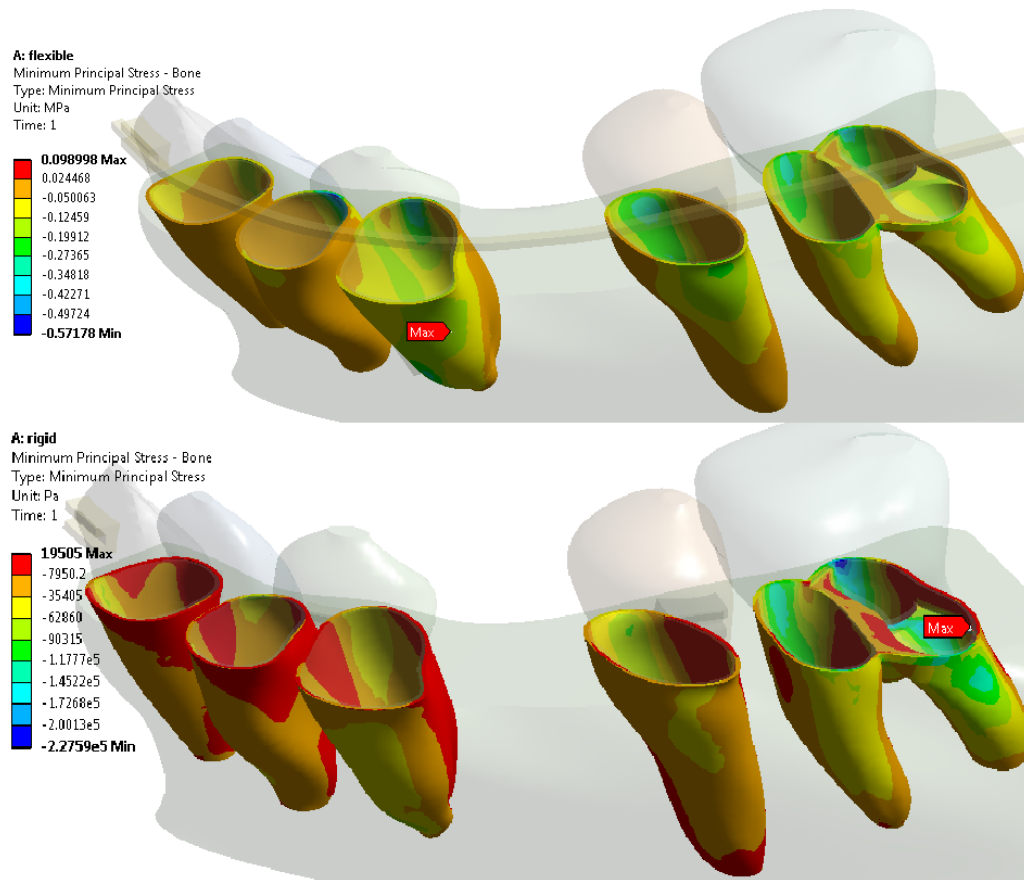


Fig. 3.7.: Comparison of third principal stress in bone from detailed model and simplified model

### 3.2.8 Comparison of Von-Mises Stress in Cortical Bone

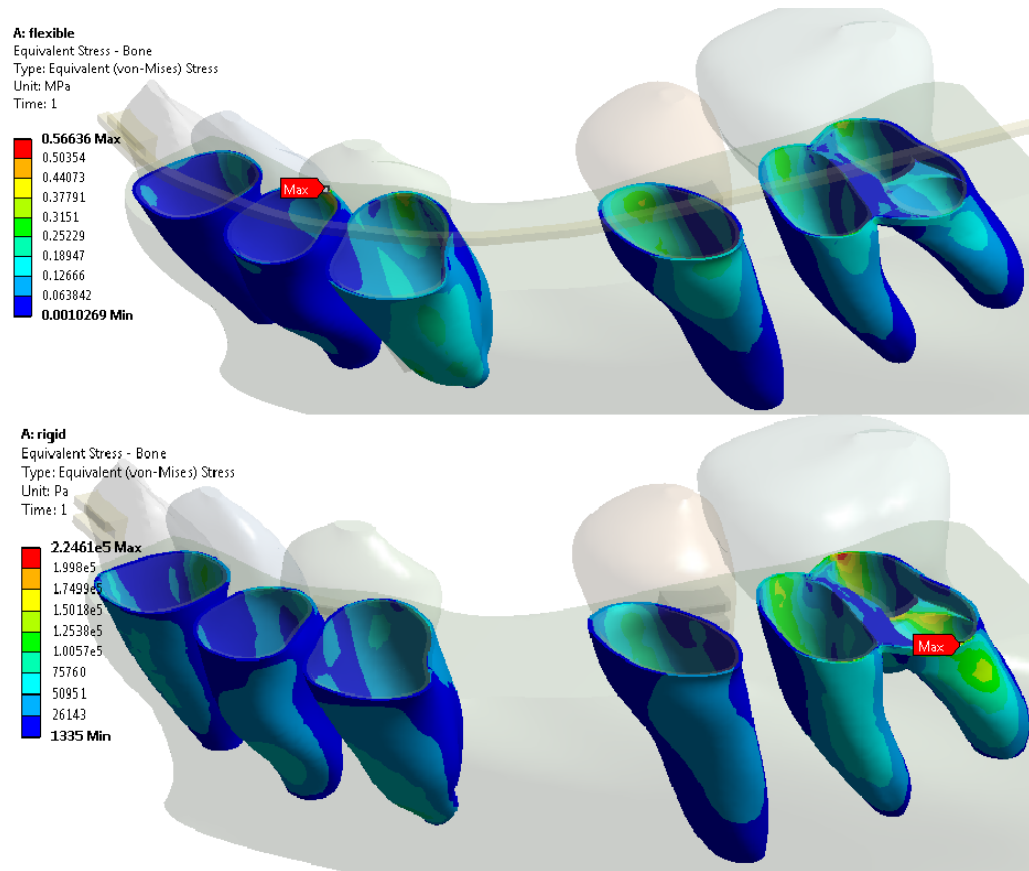


Fig. 3.8.: Comparison of Von-Mises stress in bone from detailed model and simplified model

### 3.2.9 Comparison of Tooth Displacement

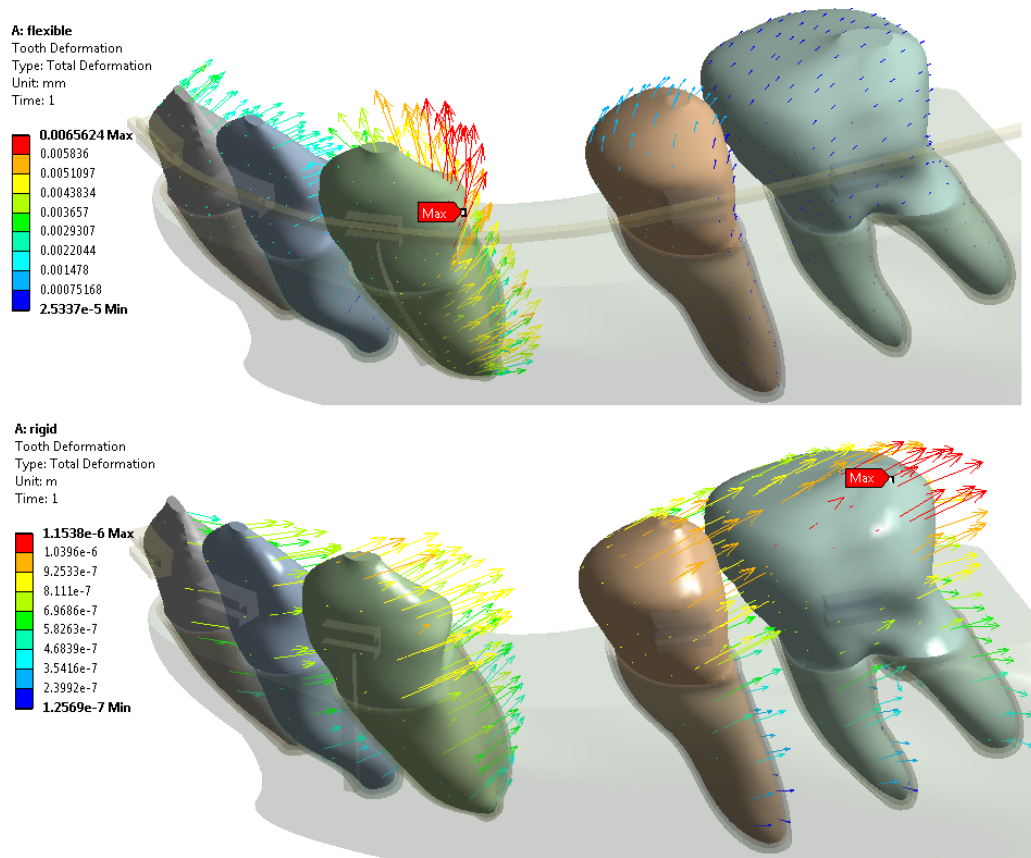


Fig. 3.9.: Comparison of tooth displacement from detailed model and simplified model

Table 3.3.: The Summary of Result Comparison from Simplified Model and Detailed Model

<b>Results</b>	<b>Maximum Magnitude</b>
1 <sup>st</sup> principal stress in PDL (detailed)	22.9KPa
1 <sup>st</sup> principal stress in PDL (simplified)	8.1KPa
2 <sup>nd</sup> principal stress in PDL (detailed)	16.9KPa
2 <sup>nd</sup> principal stress in PDL (simplified)	6.4KPa
3 <sup>rd</sup> principal stress in PDL (detailed)	15.1KPa
3 <sup>rd</sup> principal stress in PDL (simplified)	6.3KPa
Von-Mises stress in PDL (detailed)	18.3KPa
Von-Mises stress in PDL (simplified)	44.1KPa
Tooth Displacement (detailed)	0.0065mm (canine)
Tooth Displacement (simplified)	0.0011mm (molar)
1 <sup>st</sup> principal stress in Bone (detailed)	295.8KPa
1 <sup>st</sup> principal stress in Bone (simplified)	154.7KPa
2 <sup>nd</sup> principal stress in Bone (detailed)	148.8KPa
2 <sup>nd</sup> principal stress in Bone (simplified)	59.4KPa
3 <sup>rd</sup> principal stress in Bone (detailed)	571.8KPa
3 <sup>rd</sup> principal stress in Bone (simplified)	227.6KPa
Von-Mises stress in Bone (detailed)	566.3KPa
Von-Mises stress in Bone (simplified)	224.6KPa

### 3.3 OBJ #3: Mechanical Environment Changes due to Different Treatments (Canine Retraction with T-Loop and Power Arm)

For the objective #3, the tooth displacement, three principal stresses and von-Mises stress in PDL and cortical bone from three models were obtained. Figs 3.9

3.38 show the four stresses distributions and tooth displacements of the three clinical treatments. The results were investigated.

### 3.3.1 First Principal Stress in PDL from Canine T-Loop Model

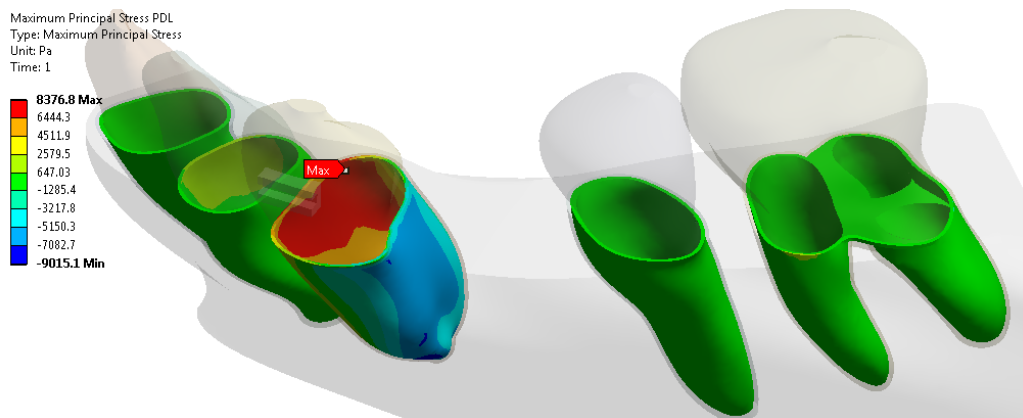


Fig. 3.10.: First principal stress in PDL from canine T-Loop model

### 3.3.2 Second Principal Stress in PDL from Canine T-Loop Model

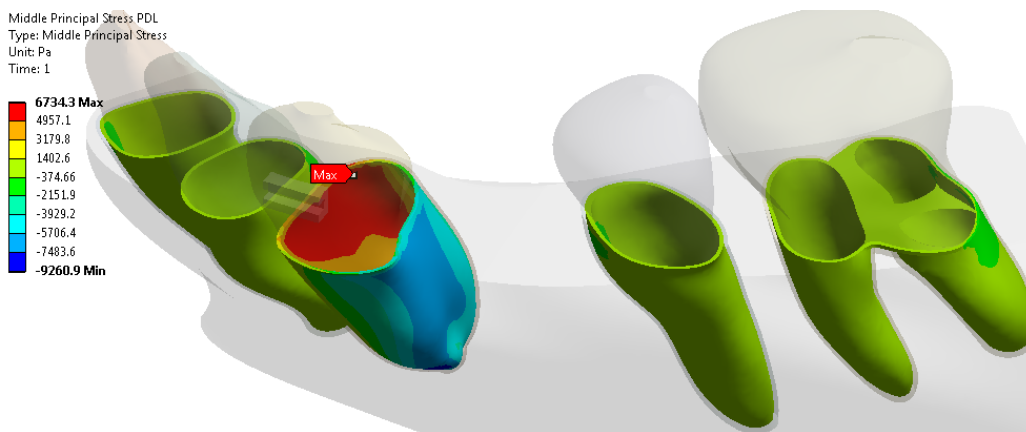


Fig. 3.11.: Second principal stress in PDL from canine T-Loop model

### 3.3.3 Third Principal Stress in PDL from Canine T-Loop Model

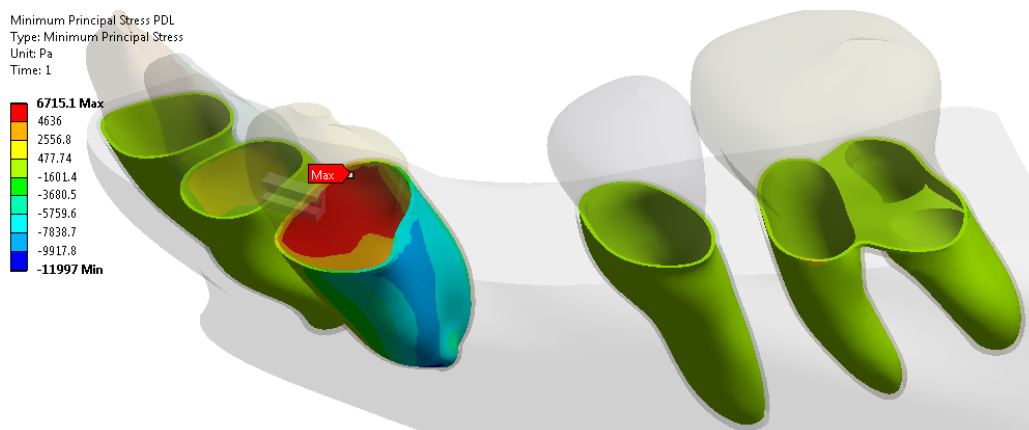


Fig. 3.12.: Third principal stress in PDL from canine T-Loop model

### 3.3.4 Von-Mises Stress in PDL from Canine T-Loop Model

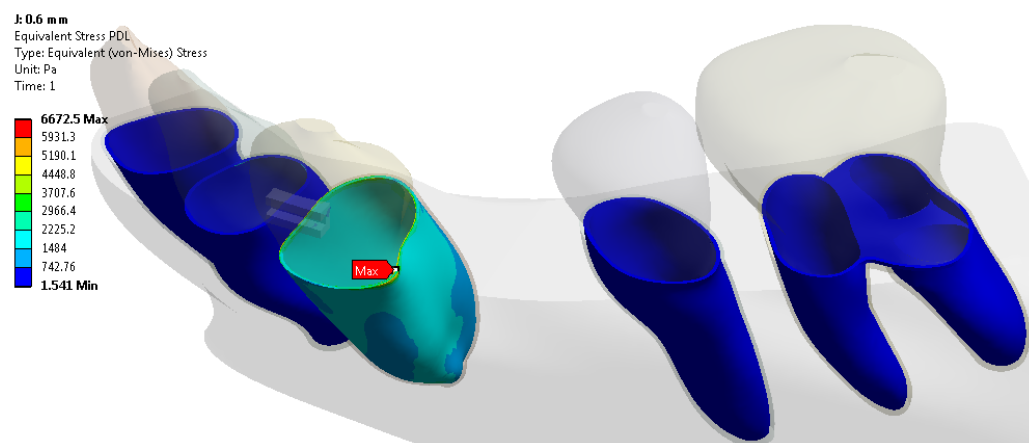


Fig. 3.13.: Von-Mises stress in PDL from canine T-Loop model

### 3.3.5 First Principal Stress in Bone from Canine T-Loop Model

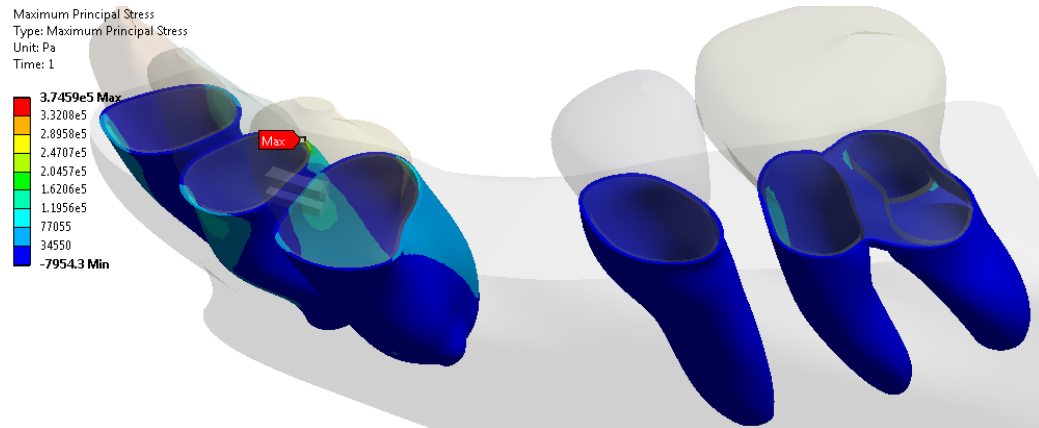


Fig. 3.14.: First principal stress in bone from canine T-Loop Model

### 3.3.6 Second Principal Stress in Bone from Canine T-Loop Model

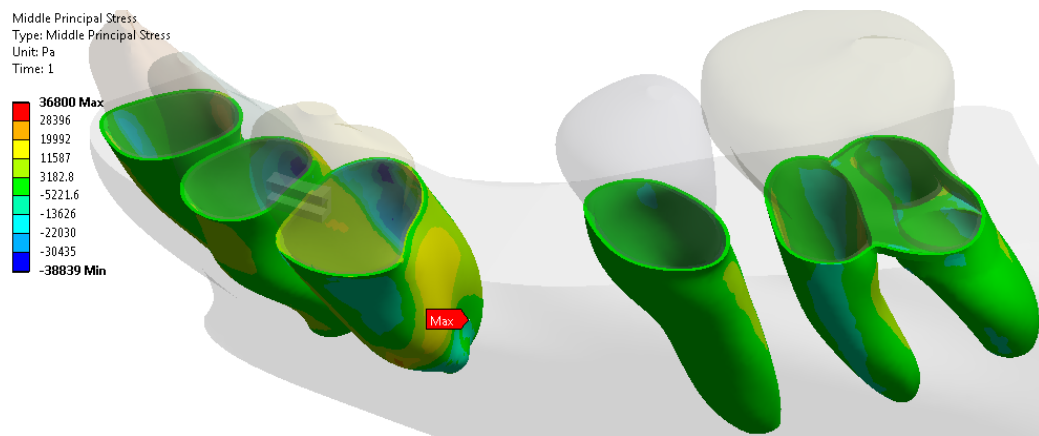


Fig. 3.15.: Second principal stress in bone from canine T-Loop model

### 3.3.7 Third Principal Stress in Bone from Canine T-Loop Model

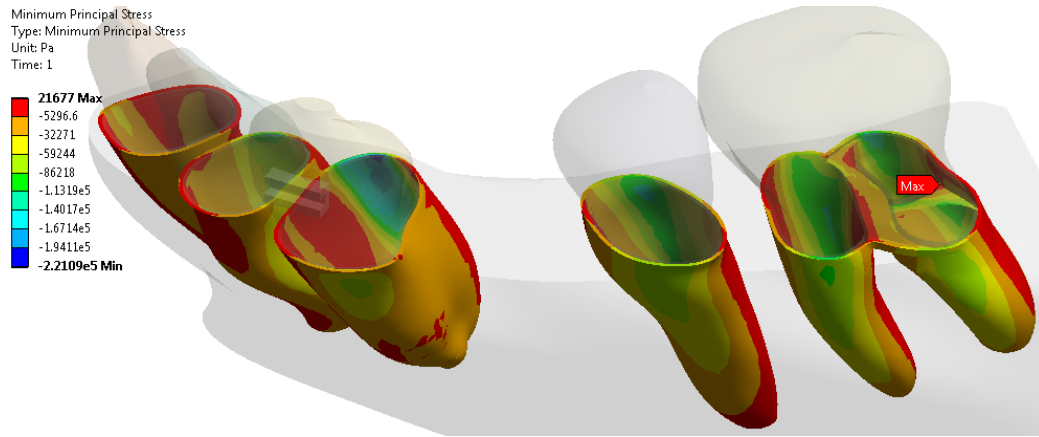


Fig. 3.16.: Third principal stress in bone from canine T-Loop model

### 3.3.8 Von-Mises Stress in Bone from Canine T-Loop Model

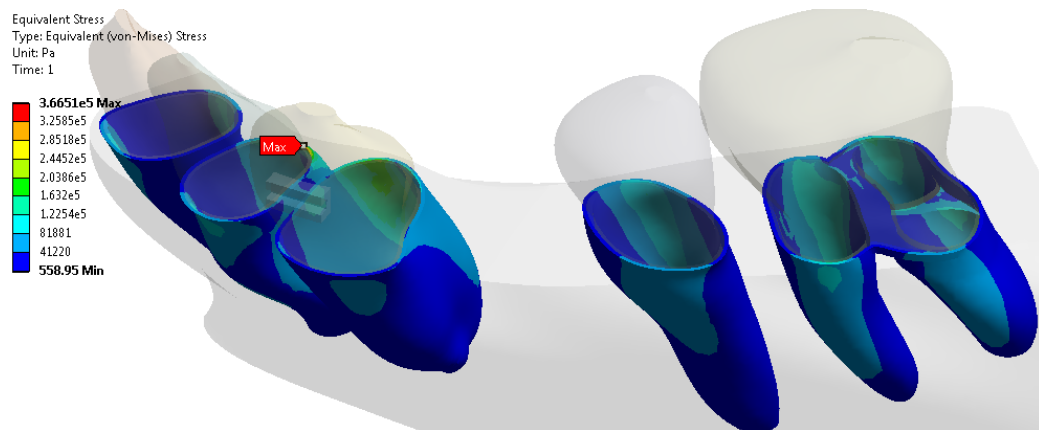


Fig. 3.17.: Von-Mises stress in bone from canine T-Loop model

### 3.3.9 Tooth Displacement from Canine T-Loop Model

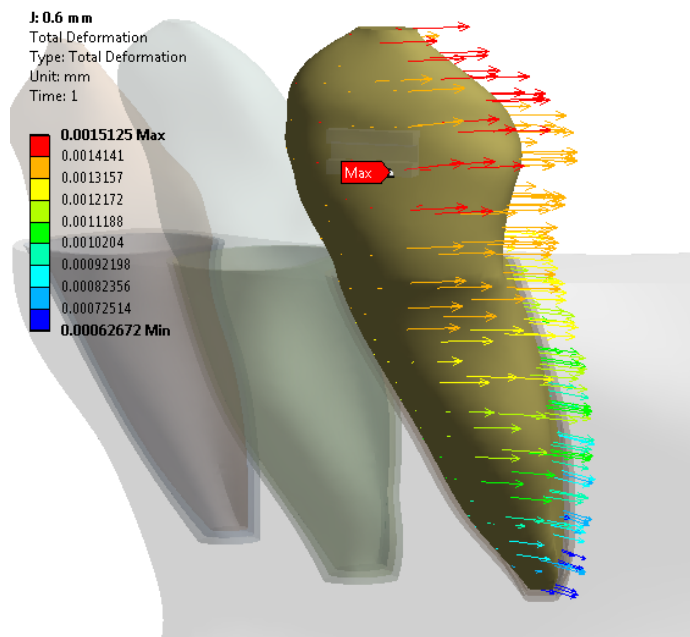


Fig. 3.18.: Tooth Displacement from canine T-Loop model

### 3.3.10 First Principal Stress in PDL from Canine Power arm Model

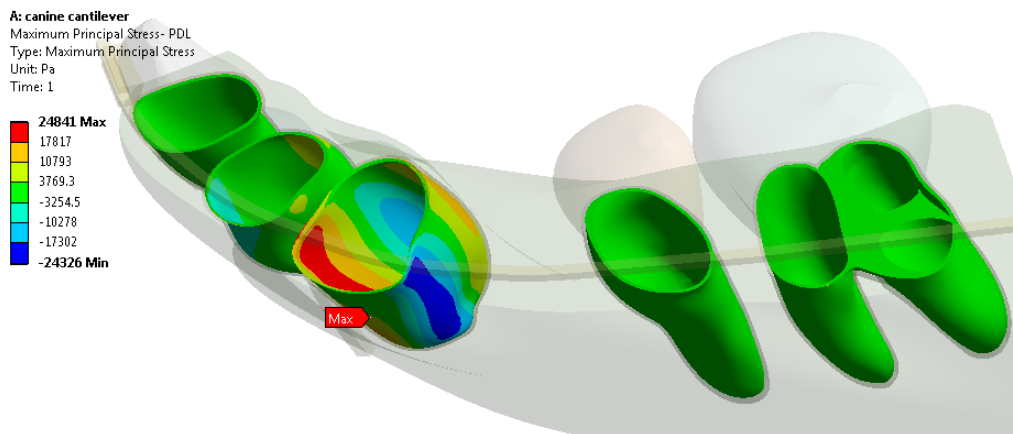


Fig. 3.19.: First principal stress in PDL from canine T-Loop model

### 3.3.11 Second Principal Stress in PDL from Canine Power Arm Model

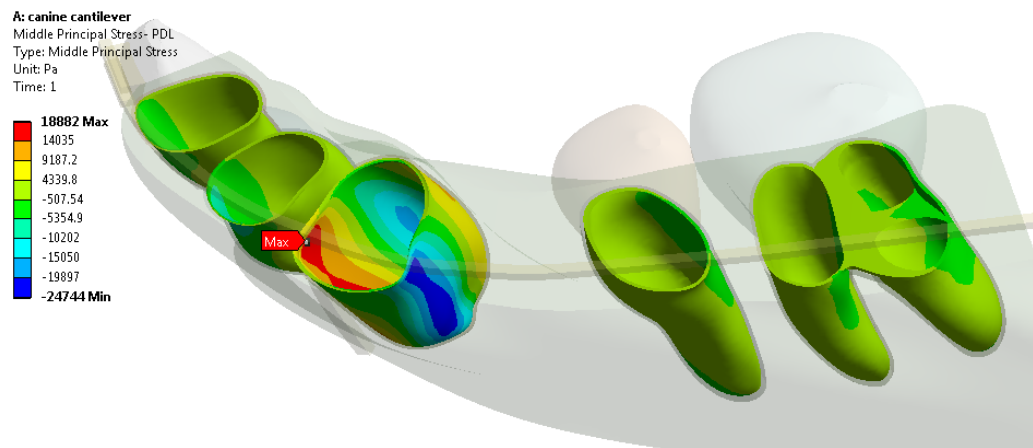


Fig. 3.20.: Second Principal stress in PDL from canine T-Loop model

### 3.3.12 Third Principal Stress in PDL from Canine Power Arm Model

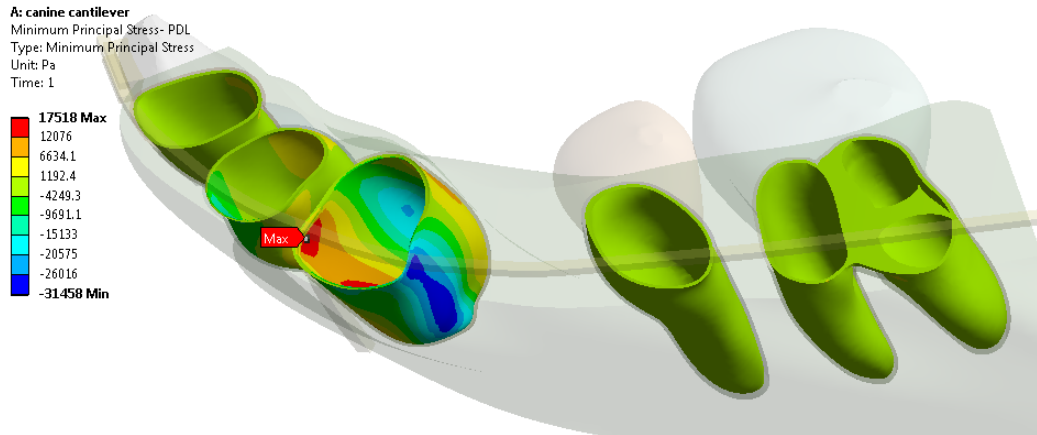


Fig. 3.21.: Third Principal stress in PDL from canine T-Loop model

### 3.3.13 Von-Mises Stress in PDL from Canine Power Arm Model

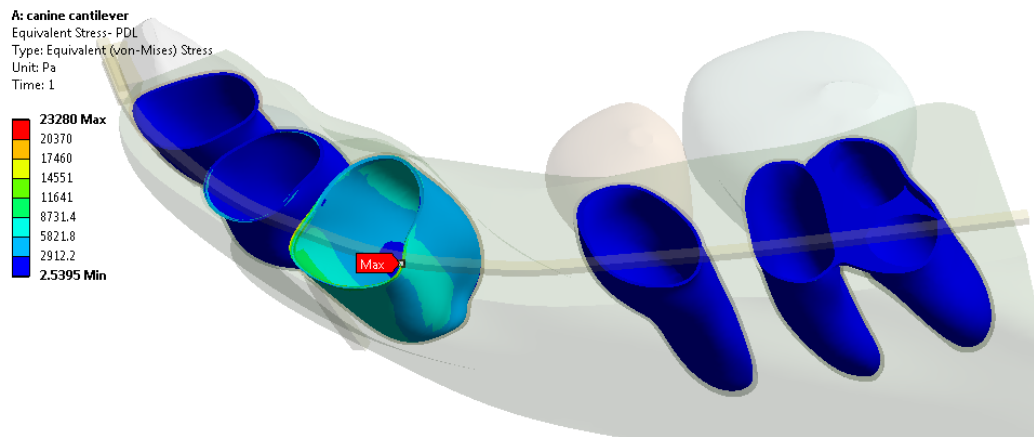


Fig. 3.22.: Von-Mises stress in PDL from canine T-Loop model

### 3.3.14 First Principal Stress in Bone from Canine Power Arm Model

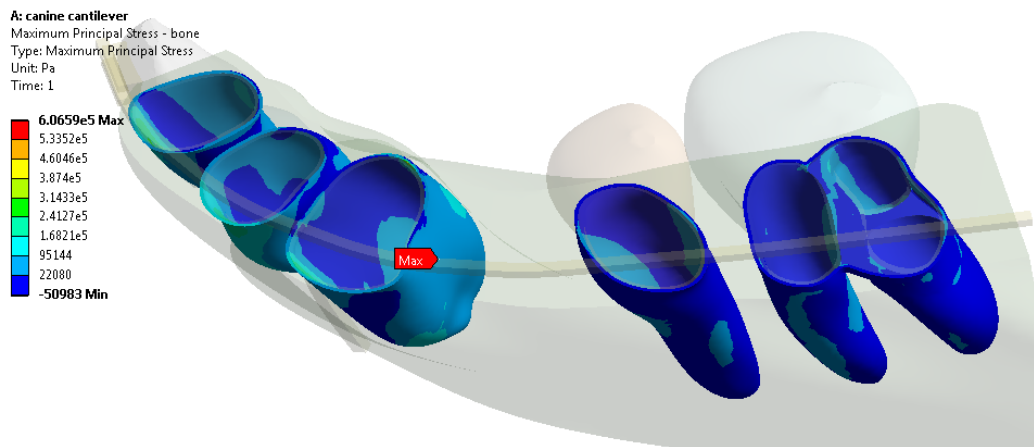


Fig. 3.23.: First principal stress in bone from canine T-Loop model

### 3.3.15 Second Principal Stress in Bone from Canine Power Arm Model

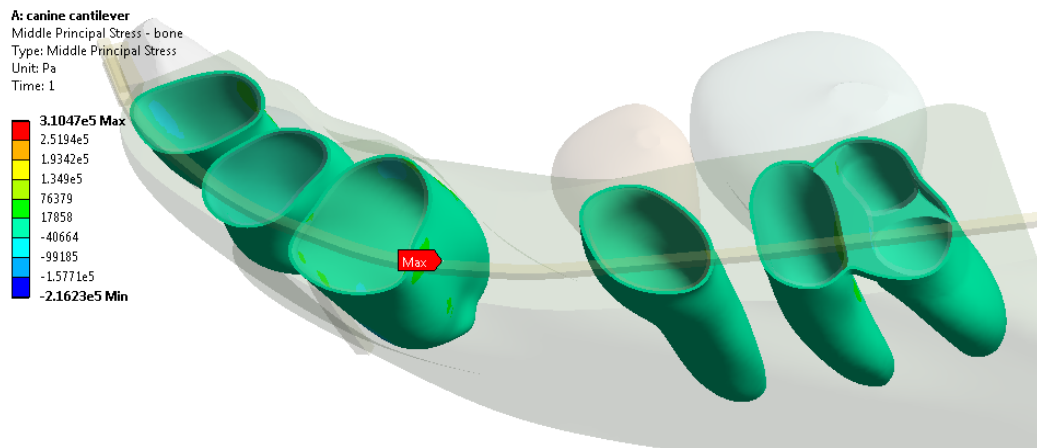


Fig. 3.24.: Second principal stress in bone from canine T-Loop model

### 3.3.16 Third Principal Stress in Bone from Canine Power Arm Model

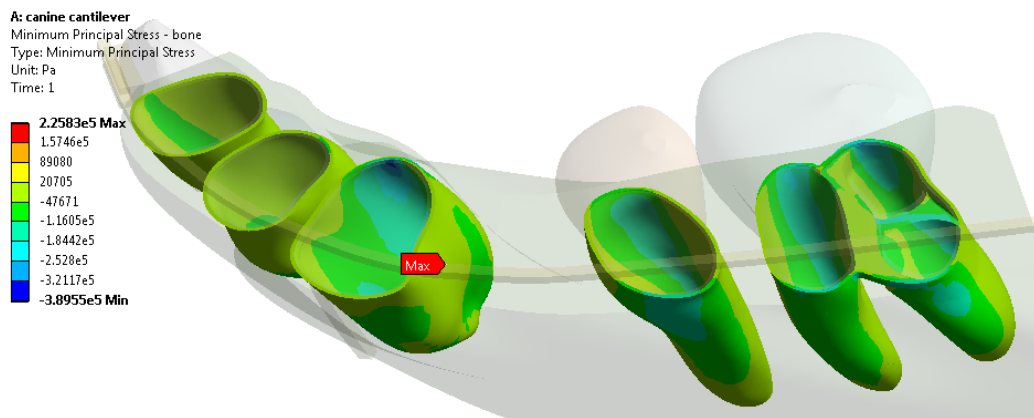


Fig. 3.25.: Third principal stress in bone from canine T-Loop model

### 3.3.17 Von-Mises Stress in Bone from Canine Power Arm Model

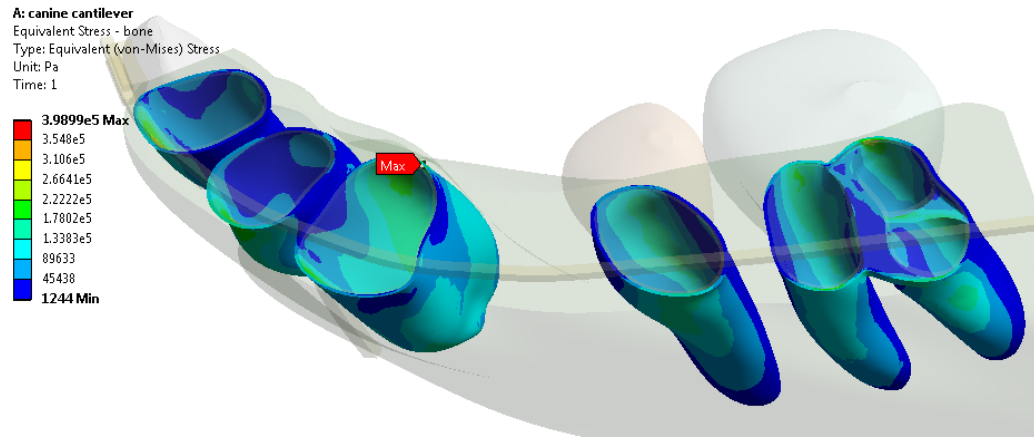


Fig. 3.26.: Von-Mises stress in bone from canine T-Loop model

### 3.3.18 Tooth Displacement from Canine Power Arm Model

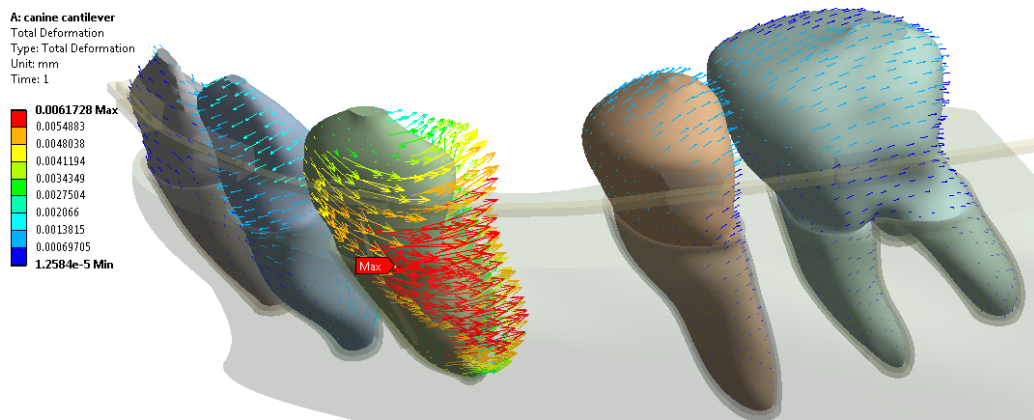


Fig. 3.27.: Tooth displacement from canine power arm model

### 3.3.19 First Principal Stress in PDL from En-masses Retraction (Power Arm on Wire) Model

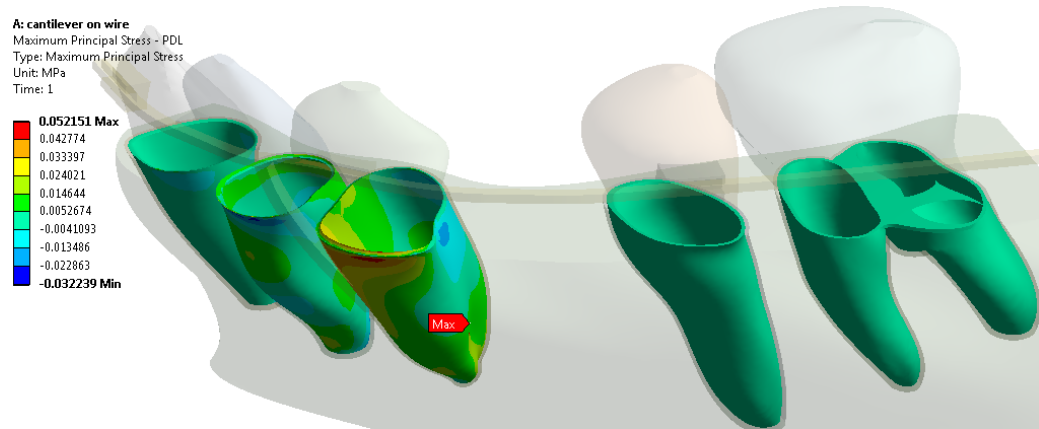


Fig. 3.28.: First principal stress in PDL from en-masses retraction (power arm on wire) model

### 3.3.20 Second Principal Stress in PDL from En-masses Retraction (Power Arm on Wire) Model

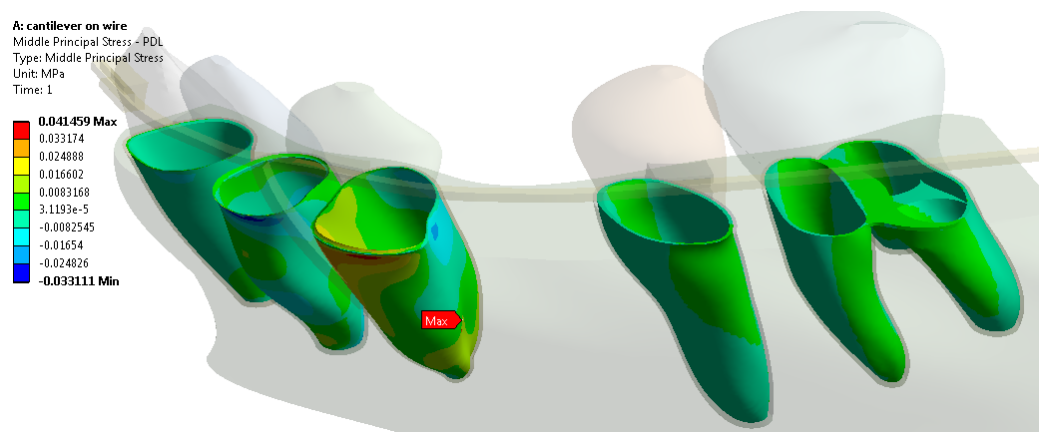


Fig. 3.29.: Second principal stress in PDL from en-masses retraction (power arm on wire) model

### 3.3.21 Third Principal Stress in PDL from En-masses Retraction (Power Arm on Wire) Model

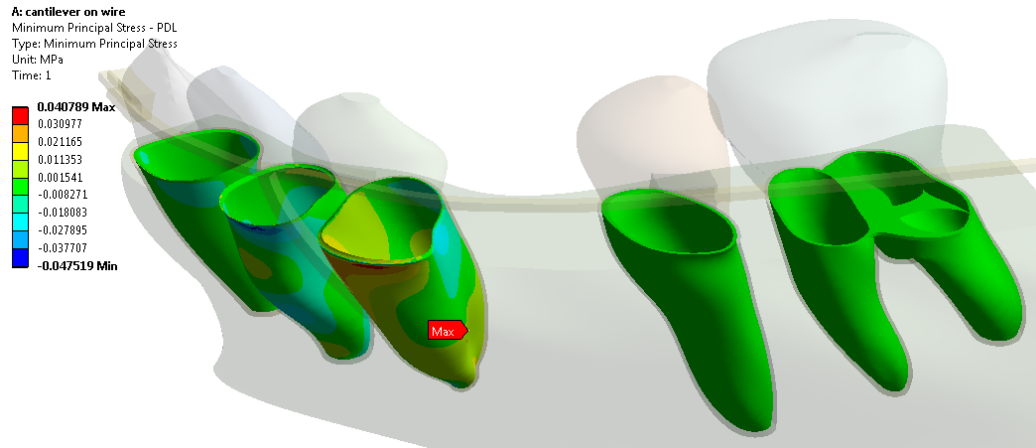


Fig. 3.30.: Third principal stress in PDL from en-masses retraction (power arm on wire) model

### 3.3.22 Von-Mises Stress in PDL from En-masses Retraction (Power Arm on Wire) Model

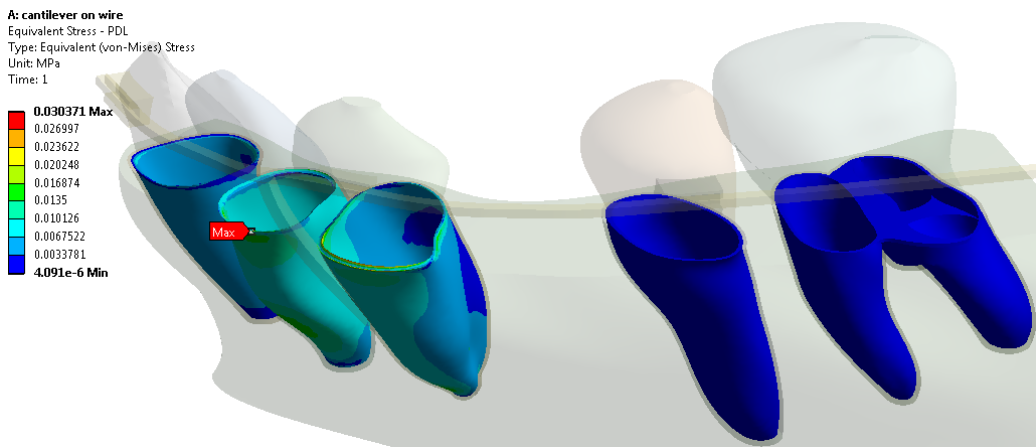


Fig. 3.31.: Von-Mises stress in PDL from en-masses retraction (power arm on wire) model

### 3.3.23 First Principal Stress in Bone from En-masses Retraction (Power Arm on Wire) Model

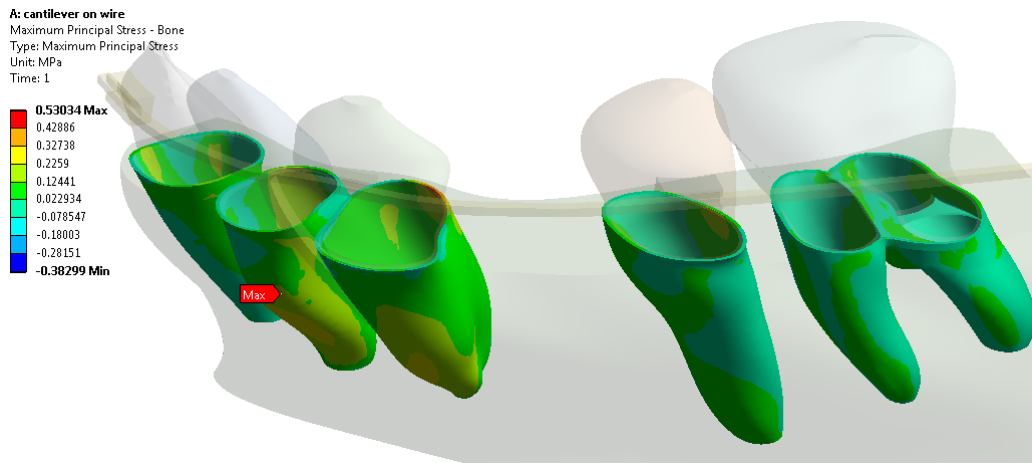


Fig. 3.32.: First principal Stress in bone from en-masses retraction (power arm on wire) model

### 3.3.24 Second Principal Stress in Bone from En-masses Retraction (Power Arm on Wire) Model

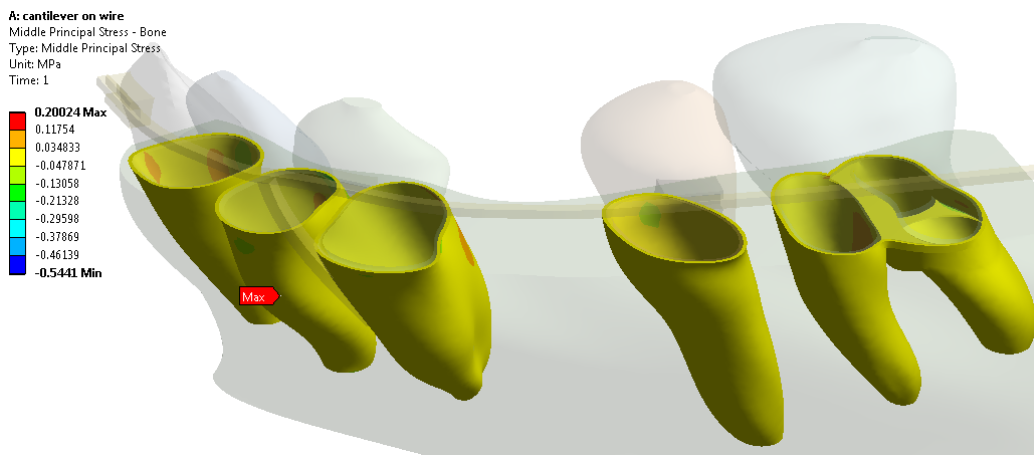


Fig. 3.33.: Second principal stress in bone from en-masses retraction (power arm on wire) model

### 3.3.25 Third Principal Stress in Bone from En-masses Retraction (Power Arm on Wire) Model

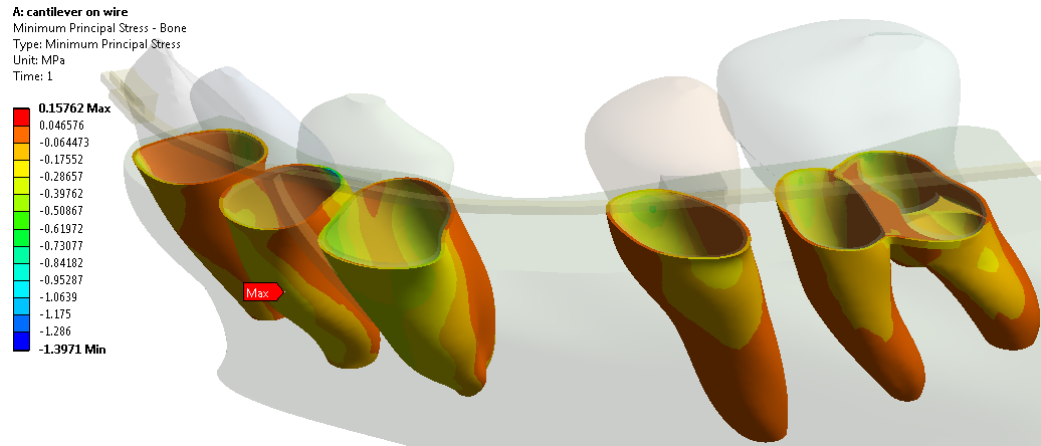


Fig. 3.34.: Third principal stress in bone from en-masses retraction (power arm on wire) model

### 3.3.26 Von-Mises Stress in Bone from En-masses Retraction (Power Arm on Wire) Model

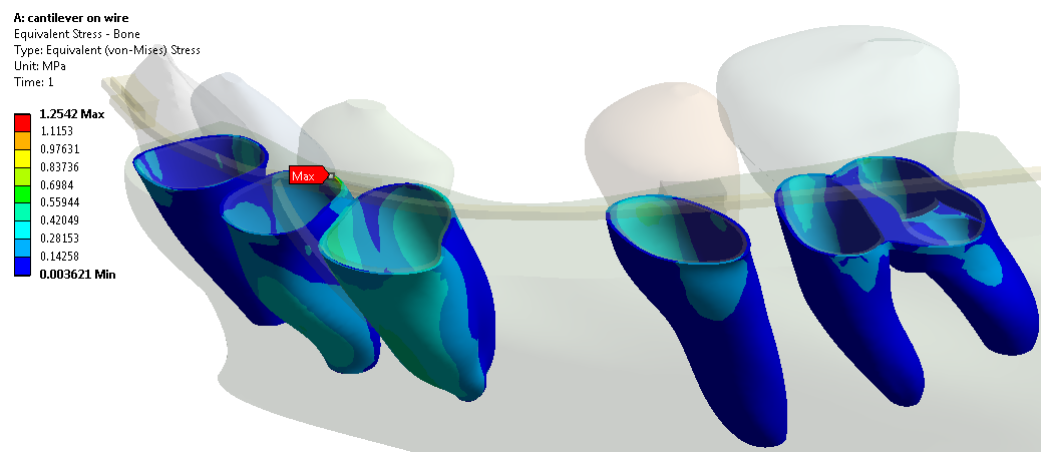


Fig. 3.35.: Von-Mises stress in bone from en-masses retraction (power arm on wire) model

### 3.3.27 Sliding Distance from En-masses Retraction (Power Arm on Wire) Model

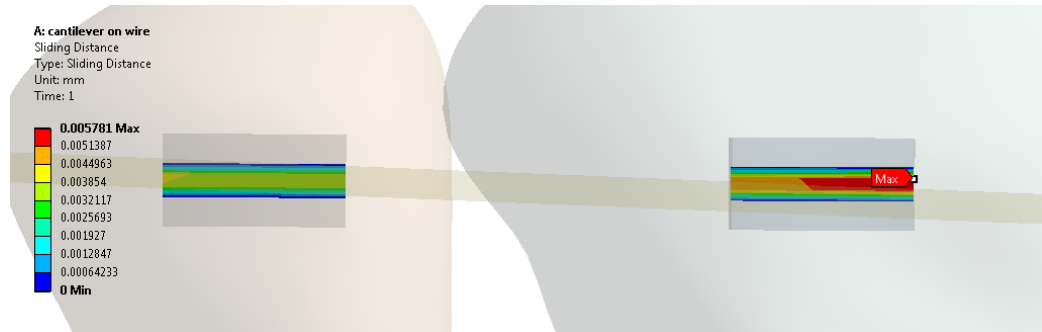


Fig. 3.36.: Sliding distance from en-masses retraction (power arm on wire) model

### 3.3.28 Tooth Displacement from En-masses Retraction (Power Arm on Wire) Model

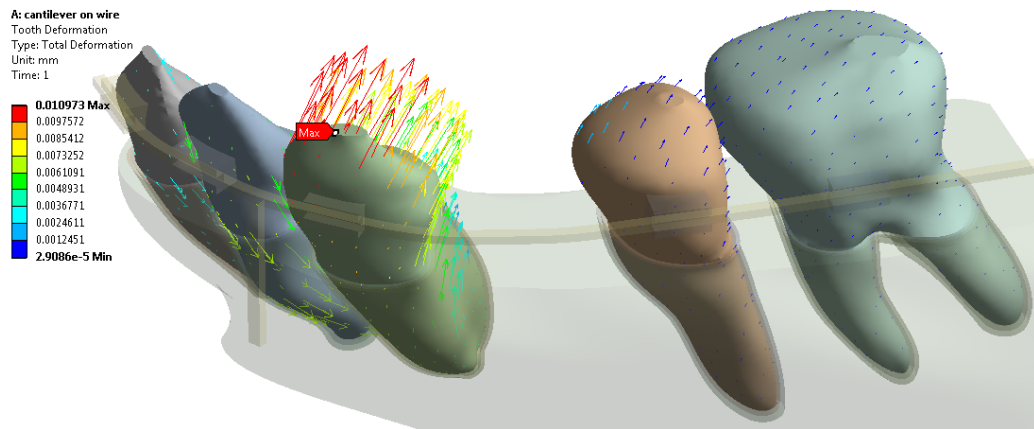


Fig. 3.37.: Tooth displacement from en-masses retraction (power arm on wire) model

### 3.3.29 Wire Displacement from En-masses Retraction (Power Arm on Wire) Model

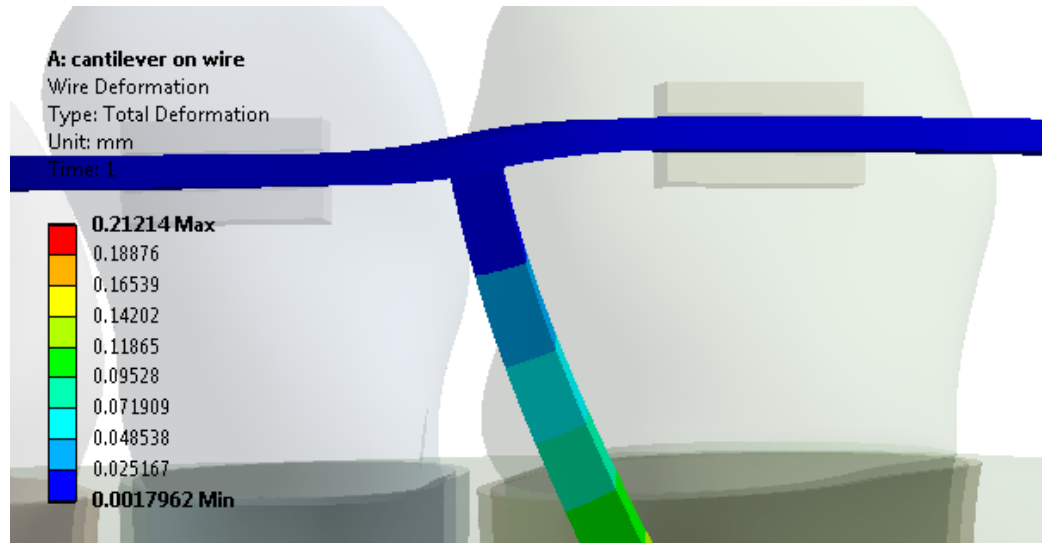


Fig. 3.38.: Wire displacement from en-masses retraction (power arm on wire) model

## 4. DISCUSSION

### 4.1 Overview

This study focused on developing a more reliable model for analyzing the ME changes due to various clinical treatment strategies. A method was developed, which modelled the mandible with details, including contact features and flexible ligations. Convergence test was done to determine the element size. Stress distributions from the simplified and detailed models were compared to see whether the simplified model can be used to replace the detailed model. Furthermore, several commonly used treatments were simulated using the new methods to determine the ME changes, which can be used for biomechanical studies and product evaluations.

### 4.2 Objective #1

The results from the convergence test showed that the model with the element size of 0.6 mm provided acceptable accuracy. The variation of the nodal displacement was about 5%, which have negligible effects on clinics. Further reducing the element size would significantly increase the computing time, but would result in negligible stress differences. Therefore the element size was used for all the models in this study.

### 4.3 Objective #2

The major differences between the simplified and the detailed model are the treatments of the interfaces that have relative motion, such as the interfaces between crown of the teeth and brackets and archwire. Previous studies modelled these interfaces using the shared nodes, meaning no relative movement allowed. These are equivalent to binding these surfaces together. The stiffness of these models are unknown. To

simulate these, the archwire connecting the teeth was modelled as rigid to simulate the binding. In these cases, the interfaces between the wire and the brackets were modelled using ANSYS bonded feature (Fig. 2.11). Although the model is not the same as those previously reported, it can demonstrate their common effects. Therefore, the major differences are still representative. The detailed model used interface elements at these interfaces. Relative movement between the surfaces is allowed. No penetration occurs. These are realistic, thus should provide more reliable results. Therefore, our objective is to compare the results from the simplified and the detailed models and see whether the new model can be replaced by the simplified model.

There are significant differences between the results of simplified model and the detailed model, not only in the magnitude of stress and displacement, but also in the stress pattern and tooth movement trends. The stress and displacement distributions from the two models are clearly different. In the comparison of von-Mises stress distribution, for example, the orthodontic load was transmitted to five teeth from the simplified model while the load was concentrated on the canine in the detailed model, which is what we expected. Therefore, distribution from the detailed model is more reasonable. The locations of maximum stresses from the two models are different. All stress components shows different patterns, including 1<sup>st</sup>, 2<sup>nd</sup>, 3<sup>rd</sup> principal stresses and von-Mises stress, meaning that the simplified model resulted in significant different results than the detailed model.

The magnitude of the stresses also showed significant difference. According to the table 3.2, the maximum von-Mises stress in the PDL from the simplified model was four times lower than in the detailed model (4.4KPa verse 18.3KPa); the 3rd principal stress showed nearly four times lower (7.7 KPa vs. 26.7 KPa); the 1st principal stress showed three times lower(8.15KPa vs. 23.46KPa). The reason is that the simplified model binds the anterior teeth together so that the orthodontic load was shared by them. However, in reality, only the canine carried most of the load in the detailed model. If the actual stress level is of interest, the detailed model should be used. For example, the capillary blood pressure was reported to be 7-10 KPa. This has been

used to guide the design of appliance that provides the pressure less than that to avoid blocking the blood supply to the region. The simplified model will result in an inaccurate estimate.

The orthodontic load was applied to the power arm through the coil spring anchored at an implant. With this treatment, the canine should have a largest displacement and the molar should be minimally affected. The tooth displacements from the two models showed significant difference. The differences occurred not only in the movement pattern but also in the displacement magnitude. The canine from the detailed model was under tipping and rotation movement and the maximum displacement was 0.0056mm at the tip of the crown. The anterior teeth in the simplified model were under a translation movement with the maximum displacement being 0.0013 mm. In addition, the posterior molar from the simplified model also had significant movement (0.0009 mm). There should be relative motion (sliding) between the archwire and brackets. The detailed model had resulted in a relative displacement of 0.0034mm maximum displacement in the 2<sup>nd</sup> premolar bracket slot.

Our study has demonstrated clearly that the simplified model cannot be used to replace the detailed model. Stress distributions and magnitudes from the two models were significantly different, meaning the results from the simplified model should not be used for stress distribution and stress quantification.

#### **4.4 Objective #3**

##### **4.4.1 Effects of Cantilever Location on the Mechanical Environment**

Sliding mechanics using power arm is common in the clinic. The power arm location varies in practice. The pros and cons have not been clearly identified. This study is the first to evaluate the ME change due to the location of the power arm. The models 3 and 5 were used for evaluating the ME difference due to the location of the power arm. Our results indicated that the power arm located on the wire between the lateral incisor and canine showed a higher stress magnitude in PDL. The

maximum compression stress from this model reached to 47.5KPa which is the higher than the maximum compression stress from the other model (power arm on bracket). The maximum 1st principal stress was 52.2KPa and it was 29.3KPa higher than the stress in the other model (22.9KPa). The maximum principal stresses in both model occurred on canine. In the von-Mises stress result (Figure 3.31), it shows that the maximum von-Mises stress (30.4KPa) occurred on the top of the PDL (lateral incisor). The von-Mises stress was concentrated on the anterior three teeth because the stress on 2nd premolar and 1st molar were relative lower (between 4 300Pa)

The displacement results showed the canines initial displacement response. In Figure 3.37, the red arrows were pointing to the lingual and occlusal directions. The displacement pattern indicated that the tooth rotated and extruded under the orthodontic load. The displacement on the crown was much larger than the displacement on the root apex which indicates tipping. The other neighboring anterior incisors had totally different movement patterns. They were intruded instead. The yellow arrows in Fig. 3.37 shows the direction of movement. The reason that caused the totally different movement of incisors and canine should be the bending and twisting of the wire. Figure 3.38 shows the deformation of the wire with a 30 times magnified display result.

#### **4.4.2 Mechanical Environment Change due to Segmental T-loop Used for Canine Retraction**

The displacement result in Figure 3.17 showed that the canine was under a combination of translation and tipping movement in this case. The maximum displacement (red) was 0.00133mm while the minimum displacement (blue) was 0.00076mm. The amount of displacement at the tip of the canine is different from the displacement at the apex, meaning a tipping occurred. The center of rotation is not at the mass center, thus both translation and tipping exist. The displacements of the buccal surface

are different from these on the lingual surface, meaning that the tooth also rotated about its long axis.

In the result of Von-Mises stress, all the stresses were concentrated on canine. The highest stress was 59.2KPa on the top of the PDL while the stress on other area of PDL was at an average of 17KPa. The stress concentration was not obvious in this treatment because there were no concentration area found in the result of the principal stresses and von-Mises stress.

In the previous study [42] which had the same orthodontic loading and similar boundary conditions, the range of the average 3rd principal stress in PDL of a canine T-Loop retraction model is from -10KPa to 8KPa. The range of the average 1st principal stress in PDL is from -6KPa to 13KPa. And the range of average Von-Mises stress in PDL is from 1.5KPa to 5KPa. While in my model, the range of 1st principal stress is from -9KPa to 8.3KPa, -12KPa to 6.7KPa for the 3rd principal stress and 1.5KPa to 6.7KPa for the Von-Mises stress. By comparing the stress results in PDL from my model and previous model, we find out that the magnitude of stresses are pretty close to each other. In my model, the maximum 3rd principal stress is 2KPa (-12KPa verse -10KPa) larger than the previous model. The maximum 1st principal stress is 4.7KPa (8.3KPa verse 13KPa) smaller than the previous model. The maximum Von-Mises stress is 1.7KPa (6.7KPa verse 5KPa) larger than the previous model while the minimum Von-Mises stresses are at the same magnitude (1.5KPa).

#### **4.4.3 Mechanical Environment Change due to En-masse Retraction (Power Arm on Canine)**

In model 3, the maximum of 1st 2nd and 3rd principal stresses in PDL were all on canine with values of 22.9KPa, 16.7KPa and 26.7KPa respectively. The maximum value of von-Mises stress in PDL was 15.6KPa located on the inner surface of PDL. The stresses on the other teeth were relative low compared with canine based on the color variation pattern (Figs. 3.1 - 3.3). The stress distribution patterns of the three

principal stresses on canine can be identified, not only the magnitudes but also the high stress locations (Figs. 3.1 - 3.3).

## 5. CONCLUSION

The objectives of this study have been achieved. The conclusions are showing below.

1. The detailed model demonstrated the stress distributions that are reasonable, thus the results are more reliable.
2. The simplified model cannot be used to replace the detailed model.
3. Clinical treatment can be simulated using the detailed model. It can be used to estimate the stress and displacement due to these treatments. Some specific conclusions are:
  - The segmental T- Loop has a better ability to translate the canine initially than power arm and power arm is better in rotating canine.
  - Power arm has bigger crown displacement of canine than T-loop.
  - Power arm creates higher maximum 3rd principle stress than T-loop.
  - The stiffness behavior of the wire can affect the results significantly and it is very critical to the stress and displacement, thus need to be modeled realistically when trying to predict the clinical outcomes.

## REFERENCES

## REFERENCES

- [1] B. Thilander, L. Pena, C. Infante, S. S. Parada, and C. de Mayorga, "Prevalence of malocclusion and orthodontic treatment need in children and adolescents in bogota, colombia. an epidemiological study related to different stages of dental development," *Eur J Orthod*, vol. 23, no. 2, pp. 153–67, 2001.
- [2] N. Joshi, A. M. Hamdan, and W. D. Fakhouri, "Skeletal malocclusion: a developmental disorder with a life-long morbidity," *J Clin Med Res*, vol. 6, no. 6, pp. 399–408, 2014.
- [3] J. Rusanen, S. Lahti, M. Tolvanen, and P. Pirttiniemi, "Quality of life in patients with severe malocclusion before treatment," *European Journal of Orthodontics*, vol. 32, no. 1, pp. 43–48, 2010.
- [4] D. P. Brunetto, E. F. SantAnna, A. W. Machado, and W. Moon, "Non-surgical treatment of transverse deficiency in adults using microimplant-assisted rapid palatal expansion (marpe)," *Dental Press Journal of Orthodontics*, vol. 22, no. 1, pp. 110–125, 2017.
- [5] G. E. Wise and G. J. King, "Mechanisms of tooth eruption and orthodontic tooth movement," *J Dent Res*, vol. 87, no. 5, pp. 414–34, 2008.
- [6] R. F. Viecilli, T. R. Katona, J. Chen, J. K. Hartsfield, and W. E. Roberts, "Three-dimensional mechanical environment of orthodontic tooth movement and root resorption," *American Journal of Orthodontics and Dentofacial Orthopedics*, vol. 133, no. 6, pp. 791.e11–791.e26, 2008.
- [7] H. Qian, J. Chen, and T. R. Katona, "The influence of pdl principal fibers in a 3-dimensional analysis of orthodontic tooth movement," *Am J Orthod Dentofacial Orthop*, vol. 120, no. 3, pp. 272–9, 2001.
- [8] L. You, S. Temiyasathit, P. Lee, C. H. Kim, P. Tummala, W. Yao, W. Kingery, A. M. Malone, R. Y. Kwon, and C. R. Jacobs, "Osteocytes as mechanosensors in the inhibition of bone resorption due to mechanical loading," *Bone*, vol. 42, no. 1, pp. 172–9, 2008.
- [9] S. D. Tan, T. J. de Vries, A. M. Kuijpers-Jagtman, C. M. Semeins, V. Elverts, and J. Klein-Nulend, "Osteocytes subjected to fluid flow inhibit osteoclast formation and bone resorption," *Bone*, vol. 41, no. 5, pp. 745–751, 2007.
- [10] N. Yoshida, P. G. Jost-Brinkmann, Y. Koga, N. Mimaki, and K. Kobayashi, "Experimental evaluation of initial tooth displacement, center of resistance, and center of rotation under the influence of an orthodontic force," *Am J Orthod Dentofacial Orthop*, vol. 120, no. 2, pp. 190–7, 2001.

- [11] S. Moin, Z. Kalajzic, A. Utreja, J. Nihara, S. Wadhwa, F. Uribe, and R. Nanda, "Osteocyte death during orthodontic tooth movement in mice," *Angle Orthod*, vol. 84, no. 6, pp. 1086–92, 2014.
- [12] R. F. Viecilli, M. H. Kar-Kuri, J. Varriale, A. Budiman, and M. Janal, "Effects of initial stresses and time on orthodontic external root resorption," *J Dent Res*, vol. 92, no. 4, pp. 346–51, 2013.
- [13] R. F. Viecilli and C. J. Burstone, "Ideal orthodontic alignment load relationships based on periodontal ligament stress," *Orthod Craniofac Res*, vol. 18 Suppl 1, pp. 180–6, 2015.
- [14] R. F. Viecilli, A. Budiman, and C. J. Burstone, "Axes of resistance for tooth movement: Does the center of resistance exist in 3-dimensional space?" *American Journal of Orthodontics and Dentofacial Orthopedics*, vol. 143, no. 2, pp. 163–172, 2013.
- [15] M. J. D. Campos, E. G. de Albuquerque, B. C. H. Pinto, H. M. Hungaro, M. A. Gravina, M. R. Fraga, and R. W. F. Vitral, "The role of orthodontic tooth movement in bone and root mineral density: A study of patients submitted and not submitted to orthodontic treatment," *Medical Science Monitor*, vol. 18, no. 12, pp. Cr752–Cr757, 2012.
- [16] M. E. R. Coimbra, N. D. Penedo, J. P. de Gouvea, C. N. Elias, M. T. de Souza Araujo, and P. G. Coelho, "Mechanical testing and finite element analysis of orthodontic teardrop loop," *American Journal of Orthodontics and Dentofacial Orthopedics*, vol. 133, no. 2, 2008.
- [17] H. Wang, J. Y. Wu, Q. Zhou, and J. Liu, "Initial stress in the periodontal membrane of maxillary first molar with different alveolar bone height by intrusion: 3-dimensional finite element analysis," *Shanghai Kou Qiang Yi Xue*, vol. 22, no. 3, pp. 247–51, 2013.
- [18] C. Verna, D. Zaffe, and G. Siciliani, "Histomorphometric study of bone reactions during orthodontic tooth movement in rats," *Bone*, vol. 24, no. 4, pp. 371–379, 1999.
- [19] H. W. Chang, H. L. Huang, J. H. Yu, J. T. Hsu, Y. F. Li, and Y. F. Wu, "Effects of orthodontic tooth movement on alveolar bone density," *Clinical Oral Investigations*, vol. 16, no. 3, pp. 679–688, 2012.
- [20] D. Schulze, M. Blessmann, P. Pohlenz, K. W. Wagner, and M. Heiland, "Diagnostic criteria for the detection of mandibular osteomyelitis using cone-beam computed tomography," *Dentomaxillofacial Radiology*, vol. 35, no. 4, pp. 232–235, 2006.
- [21] Baswaraj, M. Hemanth, Jayasudha, C. Patil, P. Sunilkumar, H. P. Raghuvver, and B. Chandralekha, "An experimental study of arch perimeter and arch width increase with mandibular expansion: a finite element method," *J Contemp Dent Pract*, vol. 14, no. 1, pp. 104–10, 2013.
- [22] S. Chen, T. M. Xu, H. D. Lou, and Q. G. Rong, "Individualized three-dimensional finite element model of facial soft tissue and preliminary application in orthodontics," *Zhonghua Kou Qiang Yi Xue Za Zhi*, vol. 47, no. 12, pp. 730–4, 2012.

- [23] A. Szucs, P. Bujtar, G. K. Sandor, and J. Barabas, "Finite element analysis of the human mandible to assess the effect of removing an impacted third molar," *J Can Dent Assoc*, vol. 76, p. a72, 2010.
- [24] C. Bourauel, L. Keilig, A. Rahimi, S. Reimann, A. Ziegler, and A. Jager, "Computer-aided analysis of the biomechanics of tooth movements," *Int J Comput Dent*, vol. 10, no. 1, pp. 25–40, 2007.
- [25] C. G. Provatidis, "A comparative fem-study of tooth mobility using isotropic and anisotropic models of the periodontal ligament. finite element method," *Med Eng Phys*, vol. 22, no. 5, pp. 359–70, 2000.
- [26] N. Yoshida, P. G. Jost-Brinkmann, Y. Koga, N. Mimaki, and K. Kobayashi, "Experimental evaluation of initial tooth displacement, center of resistance, and center of rotation under the influence of an orthodontic force," *Am J Orthod Dentofacial Orthop*, vol. 120, no. 2, pp. 190–7, 2001.
- [27] B. Melsen, "Biological reaction of alveolar bone to orthodontic tooth movement," *Angle Orthodontist*, vol. 69, no. 2, pp. 151–158, 1999.
- [28] C. Verna, M. Dalstra, and B. Melsen, "The rate and the type of orthodontic tooth movement is influenced by bone turnover in a rat model," *European Journal of Orthodontics*, vol. 22, no. 4, pp. 343–352, 2000.
- [29] N. H. Felemban, F. F. Al-Sulaimani, Z. A. Murshid, and A. H. Hassan, "En masse retraction versus two-step retraction of anterior teeth in extraction treatment of bimaxillary protrusion," *J Orthod Sci*, vol. 2, no. 1, pp. 28–37, 2013.
- [30] L. Lombardo, G. Scuzzo, A. Arreghini, O. Gorgun, Y. O. Ortan, and G. Siciliani, "3d fem comparison of lingual and labial orthodontics in en masse retraction," *Prog Orthod*, vol. 15, no. 1, p. 38, 2014.
- [31] A. Parashar, K. R. Aileni, M. R. Rachala, N. R. Shashidhar, V. Mallikarjun, and N. Parik, "Torque loss in en-masse retraction of maxillary anterior teeth using miniimplants with force vectors at different levels: 3d fem study," *J Clin Diagn Res*, vol. 8, no. 12, pp. Zc77–80, 2014.
- [32] S. Al-Sibaie and M. Y. Hajeer, "Assessment of changes following en-masse retraction with mini-implants anchorage compared to two-step retraction with conventional anchorage in patients with class ii division 1 malocclusion: a randomized controlled trial," *Eur J Orthod*, vol. 36, no. 3, pp. 275–83, 2014.
- [33] W. Heo, D. S. Nahm, and S. H. Baek, "En masse retraction and two-step retraction of maxillary anterior teeth in adult class i women. a comparison of anchorage loss," *Angle Orthod*, vol. 77, no. 6, pp. 973–8, 2007.
- [34] D. Vollmer, C. Bourauel, K. Maier, and A. Jager, "Determination of the centre of resistance in an upper human canine and idealized tooth model," *European Journal of Orthodontics*, vol. 21, no. 6, pp. 633–648, 1999.
- [35] A. Kawarizadeh, C. Bourauel, and A. Jager, "Experimental and numerical determination of initial tooth mobility and material properties of the periodontal ligament in rat molar specimens," *Eur J Orthod*, vol. 25, no. 6, pp. 569–78, 2003.

- [36] G. Pietrzak, A. Curnier, J. Botsis, S. Scherrer, A. Wiskott, and U. Belser, "A nonlinear elastic model of the periodontal ligament and its numerical calibration for the study of tooth mobility," *Comput Methods Biomech Biomed Engin*, vol. 5, no. 2, pp. 91–100, 2002.
- [37] A. N. Natali, P. G. Pavan, and C. Scarpa, "Numerical analysis of tooth mobility: formulation of a non-linear constitutive law for the periodontal ligament," *Dent Mater*, vol. 20, no. 7, pp. 623–9, 2004.
- [38] P. M. Cattaneo, T. Kofod, M. Dalstra, and B. Melsen, "Using the finite element method to model the biomechanics of the asymmetric mandible before, during and after skeletal correction by distraction osteogenesis," *Comput Methods Biomech Biomed Engin*, vol. 8, no. 3, pp. 157–65, 2005.
- [39] W. E. Roberts, R. F. Vieceilli, C. Chang, T. R. Katona, and N. H. Paydar, "Biology of biomechanics: Finite element analysis of a statically determinate system to rotate the occlusal plane for correction of a skeletal class iii open-bite malocclusion," *Am J Orthod Dentofacial Orthop*, vol. 148, no. 6, pp. 943–55, 2015.
- [40] J. Y. Tominaga, H. Ozaki, P. C. Chiang, M. Sumi, M. Tanaka, Y. Koga, C. Bourauel, and N. Yoshida, "Effect of bracket slot and archwire dimensions on anterior tooth movement during space closure in sliding mechanics: a 3-dimensional finite element study," *Am J Orthod Dentofacial Orthop*, vol. 146, no. 2, pp. 166–74, 2014.
- [41] Z. Y. Xia, F. F. Jiang, and J. Chen, "Estimation of periodontal ligament's equivalent mechanical parameters for finite element modeling," *American Journal of Orthodontics and Dentofacial Orthopedics*, vol. 143, no. 4, pp. 486–491, 2013.
- [42] Z. Xia, J. Chen, F. Jiang, S. Li, R. F. Vieceilli, and S. Y. Liu, "Load system of segmental t-loops for canine retraction," *Am J Orthod Dentofacial Orthop*, vol. 144, no. 4, pp. 548–56, 2013.